Mesoscale Modeling of Central American Smoke Transport to the United States, Part I: "Top-Down" Assessment of Emission Strength and Diurnal Variation Impacts

Jun Wang[1], Sundar A Christopher[1], U. S. Nair[1], Jeffrey S. Reid[2], Elaine M. Prins[3], James Szykman[4], Jenny L. Hand[5]

1. Department of Atmospheric Science, University of Alabama in Huntsville, 320 Sparkman Drive, Huntsville, AL, 35805

2. Aerosol and Radiation Modeling Section, Marine Meteorology Division, Naval Research Laboratory, 7 Grace Hopper Avenue, Monterey, CA, 93943

3. UW-Madison Cooperative Institute for Meteorological Satellite Studies, Madison, WI.

4. US EPA/ORD/NERL/Environmental Sciences Division, RTP, NC

5. Co-operative Institute for Research in the Atmosphere (CIRA), Colorado State University, Fort Collins, CO, 80523

Submitted to JGR-Atmospheres AIOP Special Issue
June 26, 2005.

Abstract

As is typical in this time of the year, during spring 2003 (April 20 - May21 2003), significant biomass burning smoke from Central America was transported to the southeastern United States (SEUS). A coupled aerosol, radiation and meteorology model that is built upon the heritage of the Regional Atmospheric Modeling System (RAMS) and has newly developed capabilities of Assimilation and Radiation Online Modeling of Aerosols (AROMA), was used to simulate the smoke transport and quantify the smoke radiative impacts on surface energetic, boundary layer and other atmospheric processes. This paper, the first of a two-part series, describes the model and examines the ability of RAMS-AROMA to simulate the smoke transport. Because biomass-burning fire activities have distinct diurnal variations, an hourly smoke emission inventory derived from the geostationary satellite (GOES) fire products was assimilated. In the "top-down" analysis, ground-based observations were used to evaluate the model performance, and the comparisons with model-simulated results were used to estimate emission uncertainties. Qualitatively, a 30-day simulation of smoke spatial distribution as well as the timing and location of the smoke fronts are consistent with those identified from the $PM_{2.5}$ observation network, local air quality reports, and the measurements of aerosol optical thickness and aerosol vertical profiles at the ARM SGP site in Oklahoma. Quantitatively, the model-simulated daily-average dry smoke mass near the surface correlates well with the $PM_{2.5}$ mass at 34 locations in Texas, and with the total carbon mass and non-soil potassium mass (KNON) at 3 IMPROVE sites along the smoke pathway (with linear correlation coefficients R = 0.77, 0.74 and 0.69 at the significance level larger than 0.99, respectively). The top-down sensitivity analysis indicates that the total smoke particle emission during the one-month study period is about 1.3±0.2 Tg. The results further indicate that the simulation with a *daily* smoke emission inventory provides a slightly better correlation with measurements in the downwind region in daily scales, but gives an unrealistic diurnal variation of AOT in the smoke source region. This study suggests that assimilation of emission inventories from geostationary satellite has important implications for the modeling of air quality in areas influenced by fire-related pollutants from distant sources.

1. Introduction

Central American Biomass Burning (CABB) in the Yucatan Peninsula and Southern Mexico is an important source of anthropogenic aerosols in the troposphere [*Crutzen and Andreae*, 1990]. Burning typically occurs during March – May in the tropical dry season, and ends by early June when the rainy season begins [*Crutzen et al*., 1979]. During April 20 – May 21, 2003, the Central American region was unusually dry, causing many fires to burn out of control [*Levinson and Waple*, 2004]. Under the influence of southerly winds, the emitted smoke pollutants crossed over the Gulf of Mexico and intruded deep into the southeastern United States (SEUS), thousands of kilometers from the source region. According to the Texas Commission on Environmental Quality (TECQ, http://www.tecq.state.tx.us), the transported smoke plumes severely degraded the visibility and air quality in the coastal regions along the Gulf of Mexico, and resulted in the highest mass concentrations of $PM_{2.5}$ (particulate matter with diameter less than 2.5 μm) measured in this area of Texas since the big fire event in May 1998 [*Peppler et al*., 2000; *Rogers and Bowman*, 2001]. Simulation of smoke transport driven by the accurate estimation of CABB smoke emission has important implications for the air quality forecast and assessment in this region.

In addition to degrading air quality, the long-range transported smoke aerosols also play an important role in the earth's climate system. Smoke particles, composed of sub-micron sized organic compounds are efficient at scattering sunlight as well as acting as cloud condensation nuclei [*Reid et al.*, 1998], impacting the atmospheric radiative transfer both directly and indirectly [*Twomey*, 1977; *Penner et al*., 1992]. In addition, the black carbon in smoke particles strongly absorb solar radiation [*Jacobson*, 2001], thereby enhancing atmospheric radiative heating rates, causing temperature inversions [*Robock*, 1988] and "evaporating" clouds [*Ackerman et al*., 2000; *Koren et al.*, 2004]. The radiative impacts of aerosol particles are believed to be one of the largest uncertainties in the global climate models (GCM) [*IPCC*, 2001], and are not well represented in the standard version of current meso-scale models such as the Fifth-Generation Penn State/NCAR Mesoscale Model (MM5) [*Grell et al*., 1995] or the Regional Atmospheric Modeling Systems version 4.3 (RAMS4.3) [*Harrington and Olsson*., 2001].

To simulate the smoke transport and to accurately represent smoke radiative impacts in numerical models, the smoke emission inventory must first be defined. Satellite instruments, with reliable repeat cycle and large spatial coverage, have been used widely in the last two decades to detect fires and map the columnar aerosol optical thickness (AOT) of smoke [see *Ahern et al*., 2001 and references therein]. While these satellite AOT and fire products provide critical references for the air quality monitoring and estimation of smoke emission, they are limited in describing the aerosol vertical distribution [*Kaufman et al*., 2002]. Assimilating satellite-based smoke emission inventories into the aerosol transport models is therefore a preferred method in deriving aerosol three-dimensional (3D) distributions [*Liousse et al*., 1996; *Tegen et al*., 1997; *Chin et al.*, 2002; *Park et al.*, 2003; *Uno et al.*, 2003].

The choice of aerosol transport models as well as the treatment of smoke emission in the model primarily depends on the spatio-temporal scales and physical processes of the study of interest. For climate studies, smoke emission inventories are usually estimated on the monthly or seasonal basis from polar-orbiting satellite fire products [*Ito and Penner*, 2004], and used in conjunction with global aerosol transport models [*Liousse et al*., 1996; *Chin et al*., 2002; *Park et al*., 2003]. However, mesoscale modeling and smoke inventories with finer temporal resolution are appropriate for studying the air quality and radiative impacts of smoke aerosols on regional scales [*Westphal et al*., 1991; *Jacobson et al*., 1997; *Byun and Ching*, 1999; *Trentmann et al*., 2002; *Uno et al*., 2003; *Carmichael et al*., 2003; *Colarco et al*, 2004;]. This study is the first in a two-part series and focuses on the mesoscale simulation of CABB smoke transport in the year 2003. The mesoscale model we use is a modified version of RAMS4.3 with the added capability of Assimilation and Radiation Online Modeling of Aerosols (AROMA) [*Wang et al*., 2004]. The impact of smoke on radiative processes, surface energetics and other atmospheric processes will be presented in part II of this series.

Since air quality and radiative impacts of smoke aerosols are highly dependent on the total amount of emitted smoke, the accuracy and availability of the smoke emission inventory are both important for realistically specifying the temporally varying smoke emissions in the numerical model. The accuracy of satellite-derived smoke emission inventory is affected by many highly uncertain variables (i.e. inaccurate emission factors and unknown fire numbers in

the absence of satellite observation), and is usually evaluated indirectly by comparing the model-simulated smoke (or carbon) concentration with ground-based observations (so called "top-down" method). For example, *Park et al* [2003] adjusted the satellite-based smoke emission in their model until the best agreement was achieved between modeled and measured carbon at various observation sites operated by the Interagency Monitoring of Protected Visual Environments (IMPROVE) program [*Malm et al*., 1994]. However, because their studies used a monthly smoke emission database, the impact of day-to-day variations in smoke emission on the model simulation and emission uncertainty analysis is not clear. In trying to resolve the impact of day-to-day variability of fires on the modeling of carbon monoxide (CO) from the Asian outflow, *Heald et al* [2003] used CO emission inventories with *daily* resolution, and showed little improvement when compared to the modeling results using monthly-averaged emission inventories. They attributed this to the dynamical averaging effect during the long-range transport of CO. Traditional methods of using constant smoke emission rates derived from daily or monthly smoke emission inventories may not be suitable for the simulation of CABB smoke episodes, since biomass-burnings in the tropics usually exhibit a pronounced diurnal cycle with peak emissions during early afternoon and minimum emissions at night [*Prins et al*., 1998].

This study examines the impact of including diurnal variations of fire behavior on smoke transport simulated by RAMS-AROMA. The diurnal fire behavior is specified in RAMS-AROMA by using an *hourly* smoke emission inventory from the Fire Locating and Modeling of Burning Emissions (FLAMBE) geostationary satellite database [*Reid et al*., 2004] that in turn utilizes the Geostationary Operational Environmental Satellite (GOES) Wild Fire Automated Biomass Burning Algorithm (WF ABBA) fire product [*Prins et al*., 1998]. Compared to a polar-orbiting satellite with a twice daily revisit time near the equator, GOES observations with a temporal frequency of 15 minutes have the capability to capture diurnal variations of biomass-burning fires [*Prins et al*., 1998]. We use the "top-down" approach to evaluate the FLAMBE emission uncertainties by comparing the atmospheric smoke mass concentration simulated by RAMS-AROMA to the ground-based observations. A brief description of these observation datasets and the FLAMBE smoke emission data is presented in section 2. Section 3 describes the RAMS-AROMA configuration and the experimental design of this study. An overview of the smoke events and the model simulation using the FLAMBE smoke emission values

(hereafter referred to as the baseline simulation) are presented in the section 4. Top-down sensitivity analyses of smoke emissions (including their strength and diurnal variation impact) are presented in section 5. Finally, sections 6 and 7 provide the discussion and conclusion, respectively.

2. Data and Area of Study

The area of interest in this study includes the SEUS, Mexico and the Central American region extending to the northern borders of Costa Rica (Figure 1). The datasets used in this study include: 1) Hourly smoke emissions from FLAMBE; 2) Hourly $PM_{2.5}$ mass from the U.S. EPA Aerometric Information Retrieval System Monitoring (AIRS) network; 3) Aerosol chemical composition data collected by IMPROVE [*Malm et al*., 1994]; 4) The AOT data and lidar aerosol extinction profile measured at the Atmospheric Radiation Measurement (ARM) Central Facility (36.6N, 97.5W) in the Southern Great Plain (SGP) during the intensive observation period (IOP) in May 2003.

2.1 Hourly Smoke Emission Data

Hourly smoke emission data for the study region archived in the FLAMBE database is used to specify temporally varying smoke sources in RAMS-AROMA. FLAMBE estimates smoke particle emission inventory using the emission factors outlined by *Ferek et al*. [1998] and the fire products from WF_ABBA, a dynamical contextual multi-spectral threshold algorithm that identifies fire pixels and estimates instantaneous sub-pixel fire size and temperature from GOES multi-spectral data [*Prins et al.*, 1998]. A detailed description of the FLAMBE algorithm is given in *Reid et al*, [2004; 2005a]. Currently both the WF_ABBA and FLAMBE system are quasi-operational, with fire location, instantaneous estimates of fire size, and smoke emission flux (kgm^{-2}) generated in near real time for the Western Hemisphere [*Reid et al*., 2004; http://www.nrlmry.navy.mil/flambe/].

The distribution of total smoke emitted during the time period of April 20 – May 21, 2003 shows the major emission sources located in the Yucatan Peninsula and the Manzanillo region (18N, 103W) in southern Mexico (Figure 1). In the FLAMBE database, the total smoke emission in April and May of 2003 in Central America and Southern Mexico (9N - 25N; 120W -

75W) were 0.51 Tg (1 Tg = 10^{12} g) and 0.53 Tg, respectively, and the emission during April 20 – May 21, 2003 was 0.75 Tg (as shown in Figure 1). This is the best a priori estimate of the smoke emission in the study region during this time period, and therefore is considered as a baseline emission in the model simulation. In the "top-down" analysis, the baseline emission is then adjusted by various factors until a best agreement can be found between the simulation and the observation (section 5.1). In order to derive a reasonable range for such adjustment, we first compare the baseline emission data against previous estimates in the same region but in different years.

Park et al [2003] showed that the best estimates of carbon emission in the same region in April and May 1998, were 0.85 Tg and 1.7 Tg, respectively. These estimates are equivalent to 1.2-1.7 Tg, and 2.4-3.4 Tg smoke particle emission, assuming carbon mass is about 50%-70% of the total smoke particle mass [*Reid et al.,* 2005a and references therein]. *Hao and Liu* [1994] (hereafter HL94) estimated the amount of the dry biomass being burned by fires in this region in each April in late 1970s was 39.2 Tg. Assuming the same emission factor (16g carbon per kg dry mass burned) as *Park et al* [2003], then the estimate by HL94 is equivalent to a total of 0.63 Tg carbon. The rate of deforestation in this region is estimated to have increased 0.5% per year in the 1980s and 1.2% per year from 1990 to 1995 [*FAO*, 1997]. Using these deforestation rates and the same carbon/particle mass ratio to extrapolate HL94'*s* values, it is expected that CABB smoke particle emission should be at least 1.1-1.5 Tg in a *normal* year after 1995. The extrapolated values and the estimates by *Park et al* [2003] are reasonably consistent, because CABB fire events in 1998 are the biggest CABB fire events after 1995 reported in the literature [*Peppler et al*., 2000]. The above analysis suggests that the current FLAMBE emission database most likely underestimates the total smoke emission, since the CABB fire events in 2003 are the largest since 1998. In the analysis of South American smoke emission, *Reid et al.,* [2004] also showed that a 40% underestimate of real smoke emission may exist in the FLAMBE database, because of various non-idealities in the fire products and emission algorithms. As such, in the "top-down" analysis, we increase the baseline emission by several factors ranging from 0% up to 100%.

2.2 EPA AIRS $PM_{2.5}$ Data and Smoke Coverage Report

The EPA AIRS observation network [*Watson et al*., 1998] routinely measures the hourly $PM_{2.5}$ mass concentration at more than 1500 stations across the United States. At the majority of stations, mass concentrations are measured near the surface using the Tapered-Element Oscillating Microbalance (TEOM) instruments [*Watson et al.*, 1998]. Particle-bound water included in the sampled air is removed by heating at a constant temperature (usually at 50°C) inside the instrument [*Watson et al*., 1998]. Such heating procedures, although necessary for the removal of water in the sampled $PM_{2.5}$, can also result in evaporation of semi-volatile particulate matter such volatile organic carbon and ammonium nitrate [*Allen et al*., 1997]. For this reason, the TEOM may underestimate the $PM_{2.5}$ mass by 1-2 $\mu g\ m^{-3}$ for 24 hr averages and have a larger uncertainty in the hourly $PM_{2.5}$ mass concentration [*Charron et al*, 2004; *Hitzenberger et al*., 2004]. *Allen et al.* [1997] have shown that sometimes significant, unrealistic fluctuations in the TEOM $PM_{2.5}$ mass concentration can occur over several hours, due to the change of equilibrium state of particles on the TEOM filter when ambient pollutants or moisture is changing rapidly. Nevertheless, the hourly $PM_{2.5}$ data from the TEOM instrument are sufficient to qualitatively capture the diurnal variations of $PM_{2.5}$ mass and to quantitatively measure the 24hr-average $PM_{2.5}$ mass data.

In addition to the $PM_{2.5}$ mass datasets from the EPA AIRS network, the daily report of the smoke coverage area estimated by the TECQ air quality monitoring personnel is also used as a reference to spatially map the smoke distribution for comparison to model results. These reports documented the transported CAAB smoke in Texas in April – May 2003, and an estimation of the smoke coverage area was made at 1:00pm (local time) everyday by using a combination of the ground observations as well as satellite images (http://www.tceq.state.tx.us/assets/public/compliance/monops/air/sigevents/03/event2003-04- 29txe.html).

2.3 IMPROVE Data

The IMPROVE network was initiated in spring of 1988, and consists of about 165 monitoring sites across the United States [*Malm et al.*, 1994; *Malm et al.*, 2004], of which 9 stations are located in the area of interest for the current study (see Figure. 1 and Table 1 for a list of site locations used in this study). At each site, modules are used to collect the $PM_{2.5}$ mass

on every *third* day, with a sampling duration time of 24 hours. The collected samples are then analyzed to infer the concentration of $PM_{2.5}$ mass and other trace elements such as potassium (K) and iron (Fe), as well as the major visibility-reducing aerosol species such as sulfates, nitrates, organic compounds, black (light-absorbing) carbon, and wind-blown dust [*Malm et al.*, 1994]. In this study, we use the 24 hr IMPROVE data collected in April – May 2003 for model validation, and monthly averaged IMPROVE data during 2000-2002 to derive the background concentration of carbonaceous aerosols (section 5.1).

Of particular interest is the organic carbon (OC) and black carbon (BC) concentrations as well as non-soil particulate potassium (K) from smoke measured at the various IMPROVE sites in SEUS, because these species are tracers of the smoke particles originating from biomass burning [*Kreidenweis et al*., 2001]. IMPROVE uses the thermal optical reflectance (TOR) method to analyze the concentration of OC and BC [*Chow et al.*, 1993; *Malm et al*., 1994]. Similar to other methods of measuring OC and BC, the TOR method has uncertainties from both analytical sources and artifacts [*Chow et al.*, 1993]. The uncertainty is estimated to be 15% for OC and 18% for BC, and sometimes can be up to 50% [*Chow et al*., 1993]. Although accurate separation of BC and OC is difficult, less uncertainty (7~9%) is associated with the derived total carbon (OC+BC) concentration [*Schmid et al*., 2001], and so only the total carbon mass (OC+BC) is used in this study.

Non-soil potassium in smoke particles is another indicator of biomass burning aerosols [*Kreidenweis et al*, 2001]. *Tanner et al* [2001] showed that during Central American fire events in May 1998, the K concentration in the SEUS exceeded 300% of normal mean value. However, the sources of K in the atmosphere include not only smoke but also soil. In this study, the technique of *Kreidenweis et al* [2001] is used to estimate the mass of smoke K from non-soil sources (referred to as KNON, and is equal to total K – 0.6Fe). The derived KNON data from the IMPROVE measurements are used to validate the smoke simulation from the model.

2.4 AOT and Lidar Data at the ARM SGP Site

AOT data inferred from the normal incidence multifilter radiometer (NIMFR) in the ARM SGP site (solid square in Figure 1) during the May 2003 are used to validate model

simulations. The NIMFR measures the direct solar radiation at 5 wavelengths centered at 415, 500, 615, 673, and 870 nm. AOTs are calculated based on the Beer-Lambert-Bouguer law. The calculation also includes a correction for Rayleigh scattering and ozone optical thickness. The AOT data available from the ARM data archive (http://www.archive.arm.gov/) are quality controlled with an uncertainty between 0.01 ~ 0.02.

The aerosol profiles retrieved from a Raman lidar operating at the ARM SGP site [*Ferrare et al*., 2005] are used to compare against the modeled smoke profiles. The Raman lidar measures backscattered light at the laser wavelength of 355 nm as well as the water vapor and nitrogen Raman shifted returns at 408 nm and 387 nm, respectively. The Raman technique uses the Raman nitrogen signals, and therefore has advantages in deriving the aerosol extinction (km^{-1}) profiles without making an assumption about the lidar backscatter ratio and without using AOT as a constraint [*Ferrare et al., 2001*]. Unfortunately, it was recently found that the sensitivity of Raman lidar at the ARM site has experienced a gradual loss since 2001 [*Ferrare et al*., 2005]. Hence, the Raman-lidar derived aerosol extinction profile is used qualitatively in this study to identify the location of smoke layers.

3. Model Description

The RAMS-AROMA model [*Wang et al*., 2004] is a modified version of the standard RAMS4.3 model [*Pielke et al.*, 1992] with added capabilities of modeling aerosol transport and a new radiative transfer scheme that explicitly accounts for the aerosol radiative impacts. Compared to off-line aerosol transport models, the aerosol transport model in RAMS-AROMA directly utilizes the tracer advection scheme in RAMS, and so can produce with high temporal resolution the 3D distribution of aerosols. In addition, the online transport simulation also avoids possible time lag, mismatch, and repeated computations that could occur between the offline aerosol transport and its external meteorological data sources. Since the standard version of RAMS4.3 only considers the cloud radiative effects, we replaced the original RTM [*Harriongon and Olsson*, 2001] in RAMS4.3 with an updated version of a δ-4 stream plane-parallel broadband radiative transfer model (RTM) originally developed by *Fu and Liou* [1993] to take into account the radiative impacts of both aerosol and clouds during the model simulation [*Wang et al*., 2004]. With this design, the aerosol radiative impacts are directly tied into the simulated

physical processes in the atmosphere, allowing the dynamical processes in the model to impact aerosol transport and vice versa.

The RAMS-AROMA model, initially developed by *Wang et al* [2004] to assimilate the GOES-derived AOT for the dust simulation in the Puerto Rico Dust Experiment (PRIDE), is modified in this study to assimilate a satellite-derived smoke emission inventory and to simulate the long-range transport of CABB smoke aerosols (section 3.1). During the simulation, smoke AOT is computed (section 3.2) and the smoke radiative impacts are taken into account at each model step. The different model experiments are then designed to investigate the smoke emission uncertainties and the impacts of diurnal variations in smoke emissions on the model simulation (section 3.3).

3.1 Smoke Transport and Assimilation of Smoke Emission

Smoke particles undergo such processes as condensation, coagulation, dispersion, advection, activation (as cloud condensation nuclei), and dry and wet deposition. Since smoke plumes contain hundreds of organic compounds whose individual composition and formation mechanisms are not well understood [*Turpin et al.*, 2000], the evolution of smoke physical and chemical properties is still not clear [*Gao et al.*, 2003]. What has been recognized is the rapid change of smoke properties in the first ~ 30min - 1hr after the emission [*Reid and Hobbs*, 1998], a period in which the young smoke particles dilute rapidly from a high-temperature environment into the cooler ambient atmosphere, and thus condensation and coagulation processes are expected to occur favorably [*Hobbs et al*., 2003]. If meteorological conditions allow, regional haze composed of aged smoke particles from different individual fires can be transported long distances to the downwind region. During transport, the evolution of smoke particles continues through formation of secondary organic aerosols (e.g., photochemical production and gas-to-particle conversion), oxidation of hygrocarbon compounds, as well as condensation of organic and inorganic species on the smoke particles [*Reid et al.*, 2005a].

Numerical modeling of the smoke aging process immediately after the emission [e.g., *Turco and Yu*, 1999] as well as the formation of secondary organic aerosols (SOA) in the atmosphere [e.g., *Strader et al.*, 1999; *Schell et al.*, 2001] demonstrate the need for further improvement in

the models [*see review by Kanakidou et al., 2005*]. The global and annual SOA formation estimates vary by almost a factor of 6 in different CTMs, partially because of the lack of detailed treatment of gas-particle portioning and large uncertainties (a factor of 2-5) in the estimates of SOA precursor emissions [*Kanakidou et al., 2005*]. In regional scale, several case studies have demonstrated the success of SOA simulation [*Jacobson et al*., 1997; *Zhang et al.*, 2004]. However, the initialization of these models requires the detailed and accurate chemical speciation data (such as SOA precursor emissions) that can only be possible through extensive measurements [*Jacobson et al*., 1997; *Zhang et al.*, 2004]. Indeed, direct measurements of SOAs are needed, and the current estimation of SOA relies mostly on indirect methods that are highly uncertain (see discussion by *Yu et al.*, [2004]). Furthermore, since smoke aging processes depend strongly on the burning characteristics (e.g., flaming, smoldering, fuel types, etc) and ambient meteorology of individual fires [*Reid and Hobbs*, 1998; *Hobbs et al*., 2003], it remains a challenging task to consider the aging process of smoke particles from thousands of individual fires in the Eulerian models (such as RAMS) operating on synoptic spatial scales. Therefore RAMS-AROMA assumes that the satellite-derived smoke emissions represent aged smoke particles and hence neglects the SOA formation and smoke aging process in the model. This assumption is consistent with those made in other aerosol transport models [*Westphal et al*., 1991; *Liousse et al., 1996; Chin et al., 2002; Park et al., 2003; Uno et al., 2003*]. A multi-year analysis of IMPROVE data will be used in the top-down analysis of smoke emissions to evaluate possible model uncertainties due to the lack of SOA formation in the model (section 5.1)

By neglecting SOA formation and chemical processes associated with smoke aging, the change of local smoke mass concentration is mainly due to such processes as transport, emission, dry deposition, and wet deposition:

$$\frac{\partial C}{\partial t} = \left(\frac{\partial C}{\partial t}\right)_{transport} + \left(\frac{\partial C}{\partial t}\right)_{emission} + \left(\frac{\partial C}{\partial t}\right)_{dry-deposition} + \left(\frac{\partial C}{\partial t}\right)_{wet-deposition} \quad (1)$$

In AROMA, the transport term is implemented using the generalized scalar advection framework available in RAMS [*Wang et al*., 2004]. In addition to the dry deposition by *Slinn and Slinn* [1980] over the ocean surface already present in RAMS-AROMA [*Wang et al*., 2004],

modifications have been made to include a dry deposition scheme over the land [*Zhang et al,* 2001] and a wet-deposition scheme for both wash-out [*Slinn*, 1984] and rain-out processes [*Pruppacher and Klett*, 1978]. Both dry deposition schemes include effects of gravitational settling, Brownian diffusion, and surface characteristics (surface roughness length and radius of collectors as a function of surface type and season). In the two wet deposition schemes, the deposition velocity is parameterized as a function of rain rate in the model. The smoke emission rate within a grid cell of area A (m^2) is calculated as:

$$\left(\frac{\partial C}{\partial t}\right)_{emission} = \frac{\sum_j F_j \bullet S_j}{A \bullet \Delta H \bullet \Delta t} \qquad (2)$$

where j represents jth fire within that grid; F and S are the smoke emission flux (kg m^{-2}) and fire size (m^2), respectively, both specified using the FLAMBE dataset; ΔH is the injection height (m) under which smoke particles are well mixed. Since *hourly* smoke emission is used, Δt is set to 1 hour.

It is a common practice in the aerosol transport models to uniformly distribute the smoke aerosols within ΔH so that the buoyancy caused by the heat from fires can be taken account [*Colarco et al*., 2004]. However, there is no consensus on the method of defining ΔH in the model. Prior studies suggest various values of ΔH that ranged from 2 km in gloal CTMs [*Liousse et al*., 1996; *Forster et al*., 2001; *Davison et al*., 2004] to 5-8 km in regional simulations of smoke from intensive Candadian fires [*Westphal et al*., 1991; *Colarco et al*., 2004]. Based on the observations from different filed experiments, *Lavoue et al* [2000] found that typical injection height generally follows a linear relationship (with correlation coefficient of 0.95) with the fireline intensity (I, in unit of kW m^{-1}):

$$\Delta H = a \bullet I \qquad (3)$$

where a is equal to 0.23m^2 kW^{-1}. They further showed that ΔH is usually about 2-3 km for fires in northern latitude (such as in Russian), but Canadian intensive "crown" fires usually has a mean I of 33,000 kWm^{-1}, which render a mean injection height up to 7-8 km.

The biomass burning in Central America is usually less intensive than boreal forest fires, because most burnings are made by different individual farmers for the agriculture purposes [*Kauffman et al*., 2003]. Indeed, the trees are first slashed and useful wood are removed by farmers before they are ignited [*Kauffman et al*., 2003]. As a result, the fireline intensity I of CABB fires is only in the range ~ 4000 – 7800 kW m^{-1} [*Kauffman et al*., 2003], which, based on equation (3), implies that the injection height ΔH is ~ 0.9-1.5 km. We set ΔH at the eighth layer (about 1.2km) in the model [*Wang et al*., 2004]. Sensitivity studies are carried out to examine the impact of injection height on the simulation results (section 5.2).

3.2 Modeling of Smoke Optical Properties

Smoke optical properties including mass extinction coefficient, single scattering albedo, and asymmetry factor are needed in the RAMS-AROMA to derive the smoke AOT and extinction profile from the smoke mass concentration and to compute the smoke radiative effects. In RAMS-AROMA, the smoke AOT is calculated using:

$$\tau = \sum_{i=1}^{K} (Q_i \times C_i \times f(rh_i)) \times \Delta z_i \qquad \textbf{(4)}$$

where i denotes the index for the vertical layers, K is the total number of layers in the model, C is the aerosol mass concentration (g m^{-3}), Q_{ext} is the mass extinction coefficient (m^2 g^{-1}), Δz is the layer thickness (m) and $f(rh)$ is the hygroscopic factor expressed in RAMS-AROMA as a function of relative humidity (rh) using a formula by *Kotchenruther and Hobbs* [1998]. Smoke optical properties in RAMS-AROMA are adapted from *Christopher and Zhang* [2002], and are based on Mie theory computations in which the size distribution and refractive index of smoke aerosols derived during the Smoke, Cloud and Radiation- Brazil (SCAR-B) experiment are used. The computed Q_{ext} of dry smoke aerosols is approximately 4.5 m^2g^{-1} at the wavelength of 550 nm. Although this value is consistent with the lower end of Q_{ext} reported in different literatures [see review paper by *Reid et al.*, 2005b], an underestimation of 30% is highly possible. A Q_{ext} of $5m^2g^{-1}$ was used by *Penner et al* [1992] in the box-model estimation of global smoke radiative

forcing at TOA. Recent studies also reported that the CABB smoke aerosols might have larger hygroscopicity than southern American smoke aerosols [*Kreidenweis et al.,* 2002; *Iziomon and Lohmann*, 2003] This uncertainty of Q_{ext} is considered in the analysis of our model results (section 5.1).

3.3. Experiment Design

A nested grid configuration is used in this study, with a fine grid of 62x62 points and 30 km grid spacing covering Texas, nested within a coarse grid with 48 x 48 grid points and 120 km grid spacing (Figure 1). Both horizontal grids use a stretched vertical grid of 30 points and grid stretch ratio of 1.2, with the vertical grid spacing increasing from 50 m near the surface to a maximum of 750 m higher in the atmosphere. The National Center for Environmental Prediction (NCEP) reanalysis data [*Kalnay et. al.*, 1996] at 0, 6, 12 and 18 UTC are used for initializing and specifying the temporally evolving lateral boundary conditions. In RAMS-AROMA, we select the Kuo's cumulus cloud parameterization to represent the subgrid scale cumulus convection [*Walko et al*., 1995]. The level 2.5 turbulent closure model [*Mellor and Yamada*, 1974] and Land Ecosystem Atmosphere Feedback module [*Walko et al*., 2000] are used to simulate the boundary diffusion process and air-surface interaction, respectively.

Six different simulations are considered in this study and they differ only in the treatment of biomass-burning emissions and injection height. The experiment A (section 4) uses the hourly FLAMBE baseline emissions and sets the eighth model layer as the injection height (hereafter will be referred as Layer8-Hourly-1.0E simulation, or simply baseline simulation). In experiments B and C (section 5.1), FLAMBE emissions are increased (through scaling the emission in each hour) by 50% and 100%, respectively (hereafter will be referred as Layer8-Hourly-1.5E and Layer8-Hourly-2.0E). The experiment D (section 5.2) uses the daily emissions derived from hourly FLAMBE *baseline* emissions to examine the impact of diurnal emissions on the smoke transport (hereafter Layer8-Daily-1.0E). The daily smoke emission is constructed by merging all (24) hourly *baseline* emission on a given day, and the emission rate is calculated similarly to equation (2), except that Δt is set as 24 hours. The experiment E and F are similar as baseline experiment, but set the injection height at the seventh (ΔH~1.0km) and ninth model layer (ΔH~1.4km), respectively (hereafter Layer7-Hourly-1.0E and Layer9-Hourly-1.0E). All

numerical experiments are initiated at 12 UTC on April 20 2003 and end at 12 UTC on May 21 2003.

4. Results in the Baseline Simulation

4.1 Overview and Qualitative Analysis

$PM_{2.5}$ mass measurements at various stations in Texas during April 21 – May 21, 2003 showed that the air quality in southern (Figure 2 a-b), central (Figure 2 c-e), and eastern Texas (Figure 2f) were severely degraded by the smoke events and the air quality categories ranged from moderate to unhealthy. Particularly, the air quality in southern Texas was affected by CABB smoke events almost everyday during the 30-day time period (Figure 2 a-b). The $PM_{2.5}$ mass variations shown in Figure 2 illustrate that there were four major smoke events during time frames: April 21 - April 26, April 27 - May 12, May 13 - May 17, and May 18 – May 21, respectively. In the second time frame, the $PM_{2.5}$ mass concentration started to increase on April 27, and reached the peak during May 8 – May 10 at almost all stations except those in western and northern parts of Texas (Figure 2 g-h). $PM_{2.5}$ mass concentrations in southern and central Texas stations (Figure 2 a-f) suddenly dropped about 2-3 factors on May 12, a clear sign of cessation of the 15-day long smoke pollution event. The events on May 8 – May 10 were the most severe, resulting in unhealthy air quality at most stations. Satellite images during this time period indicate large smoke plumes were continuously transported across the Gulf of Mexico, impacting the SEUS (Figure 3 a-b).

Note that CABB smoke was not observed at all stations in Texas. There was apparently less smoke (if any) being transported to the western part of Texas, as the timeline of $PM_{2.5}$ mass in this region demonstrated (Figure 2g) little consistence with that in other stations (Figure 2 a-f). The sharp spikes of $PM_{2.5}$ mass concentration in Figure 2g spanned relatively short time intervals ranging from 1 or 2 hours and were possibly caused by local emission sources. The influence of smoke events was also not obvious in the station located in northern Texas (Figure 2h) except on May 12 - May 18 when an increase in $PM_{2.5}$ mass concentrations was consistent with other stations. The area most frequently covered by smoke during this 30-day time period include the southern, central and eastern part of Texas, as well as nearby areas in Louisiana, Arkansas and

Oklahoma [*Peppler et al*., 2000]. From hereon, these areas are referred as the smoke pathway regions.

The RAMS-AROMA simulation of the largest CABB smoke episode that occurred during May 9 – May 12 2003 is depicted in Figures 3 e-h, respectively. A stable high-pressure system was centered over Florida from May 9 to May 10, building a ridge along 85°W north to 35°N (Figures 3e and 3f). Southeasterly winds in the lower troposphere associated with this system continuously transported smoke aerosols from the source regions over the Yucatan peninsula to Texas and other parts of the SEUS, which was well captured in the satellite images (Figures 3a and 3b). Optimal meteorological conditions resulted in the smoke front reaching West Virginia on May 10 (Figure 3f). The northern part of the ridge started to move westward on May 11 (Figure 3g). A low pressure system originally centered at 45°N, 103°W on May 9 (Figure 3e) moved in on May 10, and replaced the ridge on May 12 (Figure 3h). These synoptic changes shifted the winds from southeasterly flow (Figures 3e and 3f) to mainly westerly (Figure 3g) and northwesterly flow (Figure 3h) between 35°N-40°N, resulting in the retreat of smoke fronts on May 11 and May 12. The clouds associated with the low pressure system made such retreat invisible in the satellite images over the continental U.S (Figures 3c). However, such retreat can still be judged in Figure 3d that showed the majority of smoke plumes were in the southern part of Gulf of Mexico. Overall, the model-simulated spatial distribution of smoke plumes (Figures 3 e-h) over the ocean is in a good agreement with those in the satellite images (Figures 3 a-d).

Assuming that the occurrence of moderate to worse air quality over large contiguous areas is an indicator of large-scale aerosol events, the model performance is qualitatively evaluated by comparing simulations to air quality categories at various AIRS $PM_{2.5}$ stations. On May 9 and May 10, the baseline simulation indicates that the air quality in Texas, Arkansas, Kentucky and West Virginia were affected by the smoke (Figures 3e and 3f), consistent with the moderate to unhealthy air quality category (e.g., AIRS $PM_{2.5}$ mass > 15.5 $\mu g\ m^{-3}$) reported by the majority of the stations (88%) in these regions. On May 11-12, observations showed that except for the southern part of Texas, air quality in the majority of the SEUS was good, indicating that these regions were not affected by CABB smoke aerosols. These features are also simulated by the model (Figures 3g and 3h), particularly in the Texas region where the areas with modeled high

smoke concentration match well with the polluted area estimated by the local EPA agencies (denoted by red arched lines in Figure 3). Note that $PM_{2.5}$ mass measurements showed moderate air quality in New Jersey on May 10 (Figures 3e and 3f) that may potentially be related to a local emission sources.

The performance of RAMS-AROMA is further evaluated by comparing model-simulated vertical distribution of smoke to lidar-derived aerosol extinction profiles from the ARM SGP site during May 9 to May 11, 2003 time period. At 0000 UTC on May 9 2003 (local time is 5 hours behind UTC), the lidar measurements showed that the smoke layer was located in a shallow PBL within 700 m above the surface (Figure 4a). Around midnight (06UTC), the nocturnal PBL demarcated the residual layer and eventually became a 100-m shallow layer near the surface in the early morning (12 UTC, May 9), and the smoke concentration decreased during this time period (Figure 4a). The PBL height rose and reached about 1km near noon time (1500 UTC) on May 9. Associated with the increase in PBL height was the transport of smoke that enhanced the smoke concentration in the PBL. An upper-level (3-4 km above the surface) smoke layer moved into the ARM site and was entrained together with the PBL in the late afternoon (2000 UTC). At night, the PBL height decreased. High concentrations of smoke were found in the shallow PBL from 0600 UTC to 1500 UTC on the late morning of May 10 (Figure 4b), and a residual layer with low smoke concentrations can be seen from 0300 UTC to 1500 UTC on May 10. The smoke concentrations decreased and totally disappeared on May 11 (Figure 4c). The RAMS-AROMA model (Figures 4 d-f) successfully captured relative locations of each smoke layer as well as their diurnal evolution shown in Figure 4 d-f, particularly the evolution of smoke profiles from 0000 to 1500 UTC on both May 9 and May 10, and the cessation of smoke plumes on May 11. However, because of the temporal (hourly) and spatial resolution (30X30km2 and 18 vertical layers) of the model output used in the figure 4 d-f, the model results are unable to resolve the sub-grid fine structures shown in Figure4 a-c. In addition, the Rayleigh scattering and Mie scattering of background aerosols could also be important at 335nm, thus some variations in lidar-derived aerosol profile (such as low aerosol extinction coefficients at 2-3 km during 0300UTC – 1500UTC of May 9, 2003) might be caused by the inhomogeneous distribution of non-smoke aerosols.

4.2 Quantitative Analysis of Baseline Simulation

4.2.1. Comparison with $PM_{2.5}$

The spatial distribution of the linear correlation coefficient R between daily-averaged model-simulated surface smoke mass concentrations and the daily-averaged $PM_{2.5}$ mass concentrations at 36 stations in Texas (Figure 5) showed a value in the range of 0.7 – 0.9 for majority of the stations (23 out of 36). Daily-averaged $PM_{2.5}$ mass concentration that is one of EPA's standards in evaluating the daily air quality is considered in this study rather than the hourly-averaged value. The hourly $PM_{2.5}$ mass concentration could be significantly affected by local emissions such as traffic and micro-scale rapid change in meteorological conditions [*Allen et al*., 1997], factors not currently resolved in RAMS-AROMA. The daily-averaged $PM_{2.5}$ mass is less affected by these factors, and is a reasonable indicator of the smoke particle concentration during the smoke event. Comparison between hourly $PM_{2.5}$ mass and model-simulated smoke mass concentrations showed an averaged correlation coefficient around 0.55 at the 36 stations in Texas, significantly lower than 0.73 in the daily comparison (figures not shown).

High correlations (>0.7) are generally in the southern (Figures 6b and 6c), central Texas (Figure 6d) and northeastern (Figures 6e-6f) Texas. In the Dallas region (33N, 97W), about 2/3 stations have R values larger than 0.8. Low correlations exist mainly in western Texas and coastal region, in particular near the Houston area (Figure 5). Since less smoke was transported to western Texas, local emissions dominated the daily averaged $PM_{2.5}$ mass, and hence RAMS-AROMA fails to capture the variations of daily mean $PM_{2.5}$ mass in this region (Figure 6h). In the Houston area, emissions from petrochemical industries in the "ship channel area" along the bank of Galveston Bay include significant amounts of hydrocarbons [*Allen et al*., 2002]. Its large day-to-day variation is a major factor in controlling daily fluctuations of $PM_{2.5}$ mass in Houston area [*Ryerson et al*., 2003; *Tropp et al*., 1998; *Allen et al*., 2002], and so resulted in reduced correlations between simulated and observed concentrations (Figure 5). In addition, the impact of sea breeze might be also another factor that resulted in the lower correlation along the coastal regions. After removal of two $PM_{2.5}$ stations in the western tip of Texas (107E west), the overall R value in the rest of 34 stations in Texas is 0.77 (Figure 6a). Such high correlation clearly demonstrates that the daily fluctuation of $PM_{2.5}$ mass are simulated well in RAMS-AROMA, particularly along the smoke pathway region (the correlation are all at >99.99%

confidence level, Figure 6). It also indicates that long-range transported CABB smoke aerosols are the first-order contributor affecting the air quality in Texas during the study time period.

The linear relationship between daily-averaged $PM_{2.5}$ mass and modeled smoke concentration varies by station, but in general the slope is about 1.5~3 (Figures 6b-6g), except in northern and western Texas where the slope varies from 3 ~ 4.5 (Figures 6h and 6i). The slopes indicate that on average, the contribution of smoke mass to $PM_{2.5}$ mass is much larger in southern and central Texas than that in western and northern Texas, which is consistent with previous analysis of Figure 2. If we interpret the intercept in the linear equation as the concentration of background $PM_{2.5}$ mass, (e.g, aerosol mass concentration in no smoke condition), the model results suggested that the transported smoke resulted in an increase in $PM_{2.5}$ mass over background aerosols by about 25%-35% (Figure 6a).

4.2.2 Comparison with IMPROVE carbon and KNON

Various studies have shown that high concentration of both KNON and carbon are reliable indicators of smoke aerosols [*Kreidenweis et al*, 2001]. Figure 7 shows the time series of simulated smoke concentrations and measured total aerosol carbon at 9 IMPROVE sites over the SEUS. Overall, the modeled smoke concentration correlates well with measured total carbon mass and KNON at 3 IMPROVE sites along the smoke pathway, with R values of 0.66, 0.8, and 0.88 in SIKE, CACR, and UPBU stations respectively (Fig. 7G-7I); while comparisons at other sites show no significant correlations (Figures 7A-7F) possibly due to two factors. Firstly, the model indicates that there is less smoke transported to these stations. The averaged smoke concentration are less than $1\mu gm^{-3}$ in Figures 7A-7F, while all larger than $2.5\mu gm^{-3}$ in Figures 7G-7I. Therefore, for those stations not along the smoke pathway, the variations of local emission may outweigh the transported smoke and dominate the fluctuations of total carbon. Secondly, the every third-day sampling procedure employed by IMPROVE network may not sufficient enough to capture all the smoke events. For instance, there were no samplings during the smoke events on May 7-8 and May 10-11. Consequently, in the following analysis, we will mainly focus the results at SIKE, CACR, and UPBU stations, the stations that were frequently affected by the smoke events.

The comparison shows that the overall correlations of modeled smoke concentration to the KNON and total carbon at SIKE, CACR, and UPBU sites are 0.69, and 0.74 respectively (Figures 8a and 8b). Such comparisons could be influenced by several factors such as the variation of K and the carbon percentage in smoke particles from different biomass fuels. In addition, the atmospheric carbon can come from many sources, not only transported smoke particles, but also secondary production and local emissions such as biogenic sources (carbon from non-smoke sources will be referred to as background carbon). As noted by *Kreidenweis et al* [2001], the industrial pollutants in Mexico, when mixed with CABB smoke aerosols, can be transported to the SEUS, and to some extent increase the level of K and carbon in the smoke plumes. Therefore, a multi-year analysis of IMPROVE data is used in this study to investigate these uncertainties.

The average mass concentrations of $PM_{2.5}$, sulfate particles and total carbon in April and May from 2000 – 2002 at SIKE, CACR, and UPBU sites along the smoke pathway are shown in Figure 9 (hereafter these 3-year averaged values are called climatological values). The impact of upwind industrial pollution sources on the concentrations at those sites is evaluated by the comparison of the sulfate concentrations observed on smoke pollution days (as judged from modeled smoke distribution and large-scale $PM_{2.5}$ observations) with the climatological values. Compared to climatological values, the $PM_{2.5}$ mass concentrations during smoke pollution days are increased at all three sites by ~30% to 80% (Figure 9). The differences in these percentages could potentially be due to the inhomogeneous spatial distribution of smoke. As expected, the increase of $PM_{2.5}$ mass results mainly from the substantial increase of carbon (>~60%) at all three sites. Interestingly, the sulfate concentration also increased (at least >10%) at all three sites during the smoke events. This is consistent with the hypothesis of *Kreidenweis et al*. [2001] that suggests the comparison in Figure 8 could be affected by upwind industrial sources. Accurate quantification of such impacts is beyond the scope of this study, since detailed emission inventories of industrial pollution in Central America are required. Nevertheless, relatively high correlations at 3 sites along the smoke pathway indicate that the model reasonably simulates the timing and relative magnitude of the smoke distribution, even though detailed chemistry processes (such as secondary production of carbon) are not considered in this study.

5. Sensitivity Analysis of Smoke Emission

5.1 Top-down estimation of smoke emission uncertainty

Since the majority of smoke particle mass is composed of carbon, using IMPROVE carbon data to calibrate the smoke emission has recently been implemented [*e.g., Park et al.,* 2003; *Carmichael et al*., 2003]. However, to apply this method, it is necessary to first quantify the amount of background carbon at the SIKE, CACR, and UPBU sites. It should be noted that the climatological values are not the same as background values, because the transport of CABB smoke to the SEUS usually occurs at least one or two times in April – May of each year. However, observation showed that the CABB events in year 2000-2002 were less intense than the 2003 events (http://www.tecq.state.tx.us). Therefore, climatological values in Figure 9 are expected to be only slightly larger than background values. Nevertheless, the climatological values in SIKE, CACR, and UPBU sites indicate a remarkable consistence, all showing that the $PM_{2.5}$ mass is ~10μgm^{-3} among which total carbon is 2.2 μgm^{-3} (or 22%) and sulfate particle mass is ~47% (Figure 9). This consistence justify us to group the measured carbon at SIKE, CACR, and UPBU sites together in the "top-down" analysis, and to hypothesize that the averaged background carbon at these three sites during 30-day time period should be less than 2.2μgm^{-3}.

To further quantify the background carbon, a best-fit linear equation was computed between model-simulated smoke concentrations and IMPROVE total carbon concentrations at the three IMPROVE sites (Figure 8b). The intercept of the linear equation indicates that when modeled smoke concentration is zero, the background carbon is about 1.37$\mu g\ m^{-3}$ (Fig. 8d). This is consistent with the above analysis which suggests that the background carbon should be less than 2.2$\mu g\ m^{-3}$. It is also reasonably consistent with recent studies by *Russel and Allen* [2004] who, using their own independent datasets and methods, showed that in southern Texas carbon mass from primary (excluding biomass-burning emissions) and secondary sources are estimated to be in the range of 1.1 – 1.6$\mu g\ m^{-3}$ (with mean value of 1.35$\mu g\ m^{-3}$) during April - May timeframe in 2001 and 2002 (cf. Fig. 6 in *Russel and Allen* [2004]). In addition, prior studies showed that the contribution of fires to the climatolgoical values of total carbon in smoke pathway region is about 1.0$\mu g\ m^{-3}$ (e.g., figures 10 and 11 ant table 2 in *Park et al*., [2003]). Based upon these

analyses, our best estimate of averaged background carbon in these three IMPROVE sites during April-May is about 1.2μgm^{-3}.

Using this estimated background carbon mass and considering that the average total carbon mass at IMPROVE sites along the smoke pathway is approximately 2.7 μgm^{-3} (Figure 8d), we estimate that the increase of carbon by smoke aerosols is about 1.5μgm^{-3} during the smoke events in 2003. The ratio between smoke particle mass and carbon mass varies with different fuel types, burning characteristic as well as meteorological conditions. But, it is usually in the range of 1.4 - 2.0 [*Reid et al*., 2005a]. If we take the median value 1.7 as the ratio used for this study, the averaged smoke particle concentration at the 3 IMPROVE sites should be about 2.6μgm^{-3}. The model-simulated smoke mass concentration averaged at the 3 IMPROVE sites is 2.0μgm^{-3} in the baseline simulation, and becomes 3.0 μgm^{-3} and 4.0 μgm^{-3} after increasing the smoke emission by a factor of 50% and 100% in Layer8-hourly-1.5E and Layer8-houyrly-2.0E (Figures 8c and 8d), respectively. This suggests that the smoke emission is possibly underestimated by 40% in the baseline case. Note that this estimate is rather conservative. Recently, *Turpin et al*. [2000] suggested that the ratio between organic aerosols and organic carbon mass could be up to 2.3. If this is the case, the baseline emission may underestimate the true emission by 70%.

Because the above "top-down" emission analysis is based upon the surface measurements only, any errors in the modeled smoke vertical profile can result in uncertainties in the emission estimates. To further quantify the emission uncertainties, the simulated *columnar* smoke AOT are compared against the measured columnar AOTs at the ARM SGP site (Figure 10). In addition, since the background AOT in ARM SGP site is usually low [*Andrews et al*., 2004], comparisons at this site also provide an opportunity to evaluate the model performance in predicting the timing of the smoke front [*Peppler et al*., 2000]. However, it should be noted that the magnitude of model-simulated AOT is not only dependant on the total smoke emission, but also can be affected by the accuracy of smoke mass extinction coefficient and hygroscopicity formulated in the model. As discussed in section 3.2, these two factors can result in a 20% - 30% underestimation of smoke AOT. These uncertainties should be included when using measured AOT to calibrate the smoke emissions used in the model.

Simulated smoke AOT in all three experiments (baseline, Layer8-hourly-1.5E, and Layer8-hourly-2.0E) well captured the fluctuations of measured AOT (Figure 10). In particular, if we consider the increase, maximum and decrease of AOTs as indicators of the timeline of smoke events (e.g., starting, peak, and ending time), then the model-simulated timeline of smoke events (such as during May8-May12 2003) is in a good agreement with those identified from observed AOTs (the temporal differences are within 4-6 hrs at most). Note that the Angstrom exponents decreased during the smoke events, which is consistent with the results of *Andrews et al* [2004] who used 2 years of ARM datasets and showed that long-range transported smoke aerosols decrease the Angstrom exponent at the ARM site. Quantitatively, the long-term record of AOT data in ARM SGP site showed that the background AOT in this region is fairly constant around 0.1 [*Andrews et al*., 2004; also Figure 10]. The model-simulated AOT in the baseline case is always lower than the measured AOT, even after adding the background AOT of 0.1 (as shown in Figure 10). The simulated smoke AOT, with an added background AOT of 0.1, has comparable values with measured AOT, when baseline emissions are increased from 50% to 100%. In the latter case, the model almost reproduces the same time series of measured AOT on May 8 - May 10. But in all experiments, the model-simulated AOTs (after plus 0.1) underestimate the measured AOTs on May 14, 2003. Figure 10 indicates that FLAMBE emissions could underestimate the true emission by 80% ~ 100%. However, it should be noted that the difference between modeled and measure AOT could also be partially due to the 20%-30% underestimation of smoke mass extinction coefficient used in the model as well as the transported sulfate associated with CABB smoke plumes that are not considered in the modeled AOT. If this is the case, then an increase of baseline smoke emission by 50%-70% would be more reasonable.

Based on the above intercomparisons of model-simulated smoke mass and columnar smoke AOT with measured quantities, an increase in the baseline smoke emission by about 60% ± 10% provides our best estimate of smoke emissions. This increase leads to 1.3±0.2 Tg of CABB smoke particle emitted during April 20 – May 21 2003. This estimate is less than the value suggested by for *Park et al*. [2003] for smoke emission during the big fire events in May 1998, but is higher than values in the normal years (based upon the extrapolation of data from HL94).

Collaborative efforts involving numerical modeling and in situ measurements of smoke particle chemical, physical and optical properties are needed to further reduce uncertainties.

5.2. Impact of Diurnal Variations and Injection Height in Smoke Emission

Compared to baseline experiment, simulation with daily emission (Layer8-Daily-1.0E) show a slight higher correlation with measured quantities (R = 0.77 for both carbon and KNON, 0.78 for $PM_{2.5}$ in Texas, table 2) in the downwind SEUS region. Further comparisons indicate that there are 12 stations in Texas showing R larger than 0.8 between $PM_{2.5}$ and modeled smoke concentration in Layer8-Daily-1.0E simulation, larger than 7 stations in baseline simulation (Figure 11). The above analysis suggests that Layer8-Daily-1.0E seems to provide a better simulation in the downwind region, at least in the daily scale, although its simulated smoke concentration near the surface is higher than baseline experiment. The averaged smoke concentration in 34 $PM_{2.5}$ stations in Texas (not including 2 stations in Western Texas) is $3.61\mu gm^{-3}$, about 20% higher than $3.02\mu gm^{-3}$ in baseline experiment. Because IMPROVE only carries out measurement on every third day, the collocated smoke concentration in 3 IMPROVE smoke-pathway stations is $2.15\mu gm^{-3}$ in average in Layer8-Daily-1.0E experiment, only about 7% higher than $2.01\mu gm^{-3}$ in baseline experiment. The relatively higher smoke concentrations near the surface in Layer8-Daily-1.0E are due to the fact that the daily emission inventory does not capture the diurnal variations of smoke emission, particularly during the night time when there are few fires [*Prins et al*., 1998] and emission rate should be minimal (close to zero). In Layer8-Daily-1.0E experiment, the total emitted smoke amount is equally distributed in both day and night. Compared to the hourly smoke emission inventory in baseline experiment, this "equally-distributed" scheme distributes more (less) smoke during the night (daytime). Since the turbulent mixing is much weaker during the night than during the day [*Stull et al.*, 1989], the impact of distributing more smoke emission during night would lead to much higher smoke concentration near the surface, and overwhelm the impact caused by the decreased smoke emission during the daytime. As the result, the simulation with daily emission inventory provides a higher smoke concentration near the surface, even in the downwind region.

Because of the lack of hourly chemical speciation data in downwind regions, above analysis can only made in daily scales. This hampers us to draw a solid conclusion weather

diurnal variation of smoke emission in important or not in the smoke simulation. As suggested by *Heald et al* [2003], the relatively better performance of simulation using daily emission inventory could be due to the dynamical mixing during the long-range transport, which could outweigh the impact of diurnal variation of smoke emission in source region. In addition, because our daily emission inventory is build upon the hourly emission inventory derived from the GOES satellite, it has a better chance to characterize the fire distribution and emission than those daily emission inventories built from polar-orbiting satellites that view the same region only once or twice per day. In fact, the daily emission inventory derived from polar-orbiting satellite fire products can be mimicked by using the hourly emission inventory at the satellite overpassing time period (for instance 10:00am – 11:00am). In other test experiments (not shown) using an emission inventory from the hourly emission inventory at a particular time as the testbed of the daily emission inventory, we found a much poor simulation results than the baseline experiment.

Physically, the hourly smoke inventory should represent the smoke emission more realistically, and should be important in the simulating the smoke distribution near the source regions. However, the lack of aerosol measurements in the Central America makes quantitative verification of this hypothesis difficult. In this study, we only qualitatively test this hypothesis by examining the diurnal variation of simulated AOT in the smoke source region. Both satellite measurements and ground-based observations have showed that biomass-burning fires in tropics have a distinct diurnal variation with peak in the noon time [*Prins et al., 1998*; *Eck et al*., 2003] in regional and monthly scales. This diurnal cycle is essentially due to the fact that the tropical biomass-burning is made by farmers for the land clearing and agriculture purposes [*Kauffman et al*., 2003]. Farmers decide the burning activities based on the weather in the morning. If metrological condition is favorable, the burning will usually start around 10:00am, and reach the peak around 12:00-2:00pm. As a result, larger smoke AOT usually appears in the later afternoon or evening [*Eck et al*., 2003]. Shown in Figure 12 is the model-simulated smoke AOT averaged at each hour in 30days in the smoke source region (Yucatan peninsular and southern Mexico). It indicates that the baseline simulation using hourly emission can successfully produce the realistic diurnal variations of smoke AOT (e.g., larger in later afternoon and evening), while Layer8-Daily-1.0E can not. The smoke AOT in baseline simulation shows the minimum AOT of 0.13 at

10:00am and maximum AOT of 0.17 at 6:00pm, with mean AOT of 0.15 and diurnal variation of 0.04 (or ~25%). Such diurnal variation pattern and magnitude is comparable to the observations by *Eck et al* [2003] during southern African biomass burning seasons.

Two experiments, Layer7-Hourly-1.0E and Layer9-Hourly-1.0E, are conducted to investigate the impact of injection height of smoke emission on the RAMS-AROMA performance. Qualitatively, these two experiments show the similar results with baseline Layer8-hourly-1.0E experiment. Quantitative comparisons with observations are shown in table 2. Compared to the baseline experiment, the model-simulated smoke concentration showed slightly lower correlation to $PM_{2.5}$ mass concentration in Texas , IMPROVE measured carbon and KNON (R = 0.75, 0.70, and 0.63 respectively) in Layer7-Hourly-1.0E experiment, but equivalent or slightly higher correlation in Layer9-Hourly-1.0E experiment (R = 0.75, 0.72, 0.72, respectively). The difference of smoke concentrations near the surface between Layer7-Hourly-1.0E (Layer9-Hourly-1.0E) and baseline experiment is within 15% (-15%). Such differences are thereby generally smaller than the uncertainties in the smoke emission inventories, and therefore would not affect our "top-down" analysis significantly.

6. Discussion

The present study estimates the uncertainties in the FLAMBE smoke emission database by comparing the model-simulated smoke concentrations with the total carbon in areas thousands of kilometers downwind of CABB smoke emission sources. Even though the top-down approach utilized in the present study has been explored by a variety of prior research efforts [e.g., *Park et al*., 2003], there are several aspects that require further investigation, including the parameterization of smoke emissions from sub-grid scale fires and accounting for the smoke aging effects.

A common and traditional approach to ingest the smoke emission into the transport model is to compute the smoke emission rate during a time interval by assuming that smoke plumes in that time interval are distributed throughout the atmospheric column over the grid point to the injection height, with well mixed or some type of predefined (such as exponential) vertical profile. This type of *ad hoc* scheme is not expected to capture fine scale features such as sub-grid smoke plumes. At any particular time step, large model uncertainties could exist in the

smoke source region where smoke plumes from different fires are possibly in the different aging states and most likely are not mixed in a similar way as being assumed in the model. Therefore, the current scheme for the smoke assimilation can only capture the average smoke spatial and temporal distribution in the source region. However, the smoke distribution in the downwind region, due to dynamical mixing during the long-range transport, can be considered to be dominated by the quasi-equilibrated regional haze layers. It is thus expected that the traditional "injection height" approach, although having large uncertainties in specifying the instantaneous emission rate in the smoke source region, can give a reliable simulation of smoke distribution in the downwind regions, which is also indicated by the validation analysis in this study. Consequently, the "top-down" approach would be more physically-meaningful if we apply it to estimates of smoke emissions on regional scales and interpret the emission estimation from a statistical stand point (e.g., less meaningful when use it to estimate the hourly smoke emission of a single fire). In this regard, this study only gives the total smoke emission estimate for a 30-day period.

We have neglected the smoke aging processes, secondary organic aerosol formation, and biogenic emissions of organic aerosols in the model. This simplification in the model can lead to various uncertainties in the conclusions we draw from the comparison between modeled and measured quantities. We have accounted for the uncertainties arising from these neglected process through the analyses of IMPROVE data and cross-validation using different datasets (section 5.1). Further quantifying these uncertainties needs better measurements of both total carbon and secondary organic carbon as well as the improvement in modeling of secondary organic aerosols. In the end, detailed chemical speciation data in daily or even hourly scales together with a better understanding of CABB smoke microphysics (such as mass extinction coefficient and the mass budget of chemical species in smoke particles) would also benefit the top-down approach used in this study.

7. Summary

We used the RAMS-AROMA model to explore the application of an *hourly* smoke emission inventory for the numerical simulation of smoke transport at regional spatial scales and hourly-daily time scales. Comparisons against ground-based measurements suggest that RAMS-

AROMA is able to realistically simulate the smoke spatial distribution as well as the timing and the location of smoke fronts. Results also showed that the model-simulated smoke concentration well captures the fluctuations of daily-averaged $PM_{2.5}$ in Texas region (with averaged R larger than 0.76), implying that the forecasts made using the RAMS-AROMA model could potentially be a useful tool in assessing the air quality in SEUS during CABB fire seasons. Uncertainties in the smoke emission are analyzed by comparing the model-simulated smoke concentration to the measured mass of carbon aerosols. The "top-down" analysis indicates that the baseline emission inventory underestimates the smoke emission by 60%±10%, and best estimate of total emitted smoke is 1.3±0.2 Tg. It is showed in sensitivity studies that the simulation using daily smoke emission inventory provides a slightly better correlation with measurements in the downwind region in daily scales, but gives an unrealistic diurnal variation of AOT in the smoke source region. These results suggest that the assimilation of an hourly emission inventory from geostationary satellite has the unique application for the high spatiotemporal simulation of long-range smoke transport. The detailed chemical speciation data with high temporal resolutions (e.g., daily or hourly), a better understanding of smoke chemical and physical properties, as well as the modeling of smoke aging process are needed to further narrow down the uncertainties in top-down" analysis.

Acknowledgements:

This research was supported by NASA's Radiation Sciences, Interdisciplinary sciences and ACMAP programs. J. Wang was supported by the NASA Earth System Science Graduate Fellowship. The GOES WF_ABBA fire monitoring effort is supported by NOAA contract 40AANE1A4073 and by NASA's ESE Interdisciplinary Science Program through Navy subcontract No. N66001-00-C-0039. NRL participation was also supported by ONR 322. The views, opinions, and findings contained in this report are those of the author(s) and should not be construed as an official U.S. Government position, policy, or decision. The lidar and AOT data were obtained from the DOE ARM program, and we are grateful to Drs. Rich Ferrare, David Turner, Joseph Michalsky, and James Barnard for their guidance in using the data.

Reference:

Allen, G.A., C.Sioutas, P.Koutrakis, R.Reiss, F.W.Lumann, and P.T.Roberts, Evaluation of the TEOM method for measurement of ambient particulate mass in urban areas, *Journal of Air and Waste Management Association*, *47*, 682-689, 1997.

Allen, D., Gulf coast aerosol research and characterization program (Houston supersite), *progress report, submitted to Environmental Protection Agency, available at htp://www.utexas.edu/research/ceer/airquality/*, 2002.

Ackerman, A.S., O.B. Toon, D.E. Stevens, A.J. Heymsfield, V. Ramanathan, and E.J. Welton, Reduction of tropical cloudiness by soot, *Science*, *288*, 1042-1047, 2000.

Ahern, F.J., J.G. Goldammer, and C.O.J. (eds), Global and Regional Vegetation Fire Monitoring from Space: Planning an Coordinated International Effort, *SPB Academic Publishing bv, The Hague*, *303*, 2001.

Andrews, E., P.J. Sheridan, J.A. Ogren, and R. Ferrare, In situ aerosol profiles over the Southern Great Plains cloud and radiation test bed site: 1. Aerosol optical properties, *J. Geophys. Res.*, *109*, 10.1029/2003JD004025., 2004.

Byun, D.W., and J.K.S. Ching, Science algorithms of the EPA Model-3 Community Multiscale Air Quality (CMAQ) modeling system, *Rep. EPA-600/R-99/030, U.S.Eviron. Prot. Agency, U.S.Govt. Print. Off., Washington, D.C.*, 1999.

Carmichael, G.R., Y. Tang, G. Kurata, I. Uno, D.G. Streets, N. Thongboonchoo, J.-H. Woo, S. Guttikunda, A. White, T. Wang, D.R. Blake, E. Atlas, A. Fried, B. Potter, M.A. Avery, G.W. Sachse, S.T. Sandholm, Y. Kondo, R.W. Talbot, A. Bandy, D. Thorton, and A.D. Clarke, Evaluating regional emission estimates using the TRACE-P observations, *J. Geophys. Res.*, *108*, doi:10.1029/2002JD003116., 2003.

Charron, A., R.M. Harrison, S. Moorcroft, and J. Booker, Quantitative interpretation of divergence between PM10 and PM2.5 mass measurement by TEOM and gravimetric (Partisol) instruments, *Atmospheric Enviroment*, *38*, 415-423, 2004.

Chin, M., P. Ginoux, S. Kinne, O. Torres, B.N. Holben, B.N. Duncan, R.V. Martin, J.A. Logan, A. Higurashi, and T. Nakajima, Troposphere aerosol optical thickness from the GOCART model and comparisons with satellite and sun photometer measurements, *J. Atmos. Sci.. 59*, 461-483, 2002.

Chow, J.C., J.G. Watson, L.C. Prichett, W.R. Pierson, C.A. Frazier, and R.G. Purcell, The DRI thermal/optical reflectance carbon analysis system: description, evaluation, and applications in U.S. air quality studies, *Atmos. Environ*, *27*, 1185-1201, 1993.

Christopher, S.A., and J. Zhang, Daytime variation of shortwave direct radiative forcing of biomass burning aerosols from GOES 8 imager, *J. Atmos. Sci.*, *59*, 681-691, 2002.

Crutzen, P.J., L.E. Heidt, J.P. Krasnec, W.H. Pollock, and W. Seiler, Biomass burning as a source of atmospheric gases CO, H2 , N2O, NO, CH3Cl and COS, *Nature*, *282*, 253-256, 1979.

Crutzen, P.J., and M.O. Andreae, Biomass burning in the tropics: Impact on atmospheric chemistry and biogeochemical cycles, *Science*, *250*, 1669-1678, 1990.

Colarco, P.R., M.R. Schoebert, B.G. Doddridge, L.T. Marufu, O. Torres, and E.J. Welton, Transport of smoke from Canadian forest fires to the surface near Washington, D.C.: Injection height, entrainment, and optical properties, *109*, doi:10.1029/2003JD004248, 2004.

Davison, P.S., D.L.Roberts, R.T.Arnold, and R.N.Colvile, Estimating the direct radiative forcing due to haze from the 1997 forest fires in Indonesia, *J. Geophys. Res.*, *109*, doi:10.1029/2003JD004264, 2004.

Eck, T.F., B.N. Holben, D.E. Ward, M.M. Mukelabai, O. Dubovik, A. Smirnov, J.S. Schafer, N.C. Hsu, S.J. Piketh, A. Queface, J.L. Roux, R.J. Swap, and I. Slutsker, Variability of biomass burning aerosol optical characteristics in southern Africa during the SAFARI

2000 dry season campaign and a comparison of single scattering albedo estimates from radiometric measurements, *J. Geophys. Res.*, *108*, doi:10.1029/2002JD002321, 2003.
FAO, State of the world's forest 1997, *Food and Agric. Organ. of the United Nations, Rome, Italy*, 1997.
Ferek, R.J., J.S. Reid, P.V. Hobbs, D.R. Blake, and C. Liousse, Emission factors of hydrocarbons, halocarbons, trace gases and particles from biomass burning in Brazil, *J. Geophys. Res.*, *103*, 32,107-32,118, 1998.
Ferrare, R., D.D.Turner, L.A.Heilman, W.Feltz, O.Dubovik, and T.Tooman, Raman lidar measurements of the aerosol extinction-to-backscatter ratio over the southern great plains, *J. Geophys. Res.*, *106*, 20,333-20,347, 2001.
Ferrare, R., D. Turner, M.Clayton, B.Schmid, J.Redemann, D.Covert, R.Elleman, J.Ogren, E.Andrews, J.Goldsmith, and H.Jonsson, Raman Lidar measurements of aerosols and water vapor over the southern great plains during the May 2003 Aerosol IOP, *J. Geophys. Res.*, *submitted*, 2005.
Forster, C., U. Wandinger, G. Wotawa, J. P, I. Mattis, D. Althausen, P. Simmonds, S. O'Doherty, S.G. Jennings, C. Kleefeld, J. Schneider, T. Trickl, S. Kreipl, H. Jager, and A. Stohl, Transport of boreal fire emissions from Canada to Europe, *J. Geophys. Res.*, *106*, 22,887-22,906, 2001.
Fu, Q., and K.N. Liou, Parameterization of the radiative properties of cirrus clouds, *J. Atmos. Sci.*, *50*, 2008-2025, 1993.
Gao, S., D.A.Hegg, P.V.Hobbs, T.W.Kirchstetter, B.I.Magi, and M.Sadilek, Water-soluble organic components in aerosols associated with savanna fires in southern Africa: identification, evolution, and distribution, *J. Geophys. Res.*, *108*, doi:10.1029/2002JD002324, 2003.
Grell, G.A., J. Dudhia, and D. Stauffer, A Description of the Fifth-Generation Penn State/NCAR Mesoscale Model (MM5), NCAR/TN-398+STR, 122pp, 1995, available at http://www.mmm.ucar.edu/mm5.
Hao, W.M., and M.-H. Liu, Spatial and temporal distribution of tropical biomass burning, *Global Biogeochemical Cycles*, *8*, 495-503, 1994.
Harrington, J.Y., and P.Q. Olsson, A method for the parameterization of cloud optical properties in bulk and bin microphysical models. Implications for arctic cloudy boundary layers, *Atmospheric Research*, *57*, 51-80, 2001.
Heald, C.L., D.J. Jacob, P.I. Palmer, M.J. Evans, G.W. Sachse, H.B. Singh, and D.R. Blake, Biomass burning emission inventory with daily resolution: Application to aircraft observations of Asian outflow, *J. Geophys. Res.*, *108*, doi:10.1029/2002JD003082, 2003.
Hitzenberger, R., A.Berner, Z.Galambos, W.Maenhaut, J.Cafmeyer, J.Schwarz, K.Muller, G.Spindler, W.Wieprecht, K.Acker, R.Hillamo, and T.Makela, Intercomparison of methods to measure the mass concentration of the atmospheric aerosol during INTERCOMP2000 - influence of instrumentation and size cuts, *Atmospheric Enviroment*, *38*, 6467-6476, 2004.
Hobbs, P.V., P.Sinha, R.J.Yokelson, T.J.Christian, D.R.Blake, S.Gao, T.W.Kirchstetter, T.Novakov, and P.Pilewskie, Evolution of gases and particles from a savanna fire in South Africa, *J. Geophys. Res.*, *108*, doi:10.1029/2002JD002352, 2003.
IPCC, Climate Change 2001: The Scientific Basis: Contribution of Working Group I to the Third Assessment Report of the Intergovernmental Panel on Climate Change, *[Houghton, J. T., Y. Ding, D. J. Griggs, M. Noguer, P. J. van der Linden, X. Dai, K. Maskell, and C. A.*

Johoson (eds)], Cambridge University Press, United Kingdom and New York, NY, USA, 881pp., 2001.
Ito, A., and J.E. Penner, Global estimates of biomass burning emissions based on satellite imagery for the year 2000, *J. Geophys. Res.*, *109*, doi:10.1029/2003JD004423, 2004.
Iziomon, M.G., and U. Lohmann, Optical and meteorological properties of smoke-dominated haze at the ARM southern greate plains central facility, *Geophys. Res. Lett.*, *30*, doi:10.1029/2002GL016606, 2003.
Jacobson, M.Z., Development and application of a new air pollution modeling system Part II: Aerosol module structure and design,, *Atmos. Environ.*, *31A*, 131 - 144, 1997.
Jacobson, M.Z., Strong radiative heating due to the mixing state of black carbon in atmospheric aerosols, *Nature*, *409*, 695-697, 2001.
Kalnay, E., M. Kanamitsu, R. Kistler, W. Collins, D. Deaven, L. Gandin, M. Iredell, S. Saha, G. White, J. Woolen, Y. Zhu, M. Chelliah, W. Ebisuzaki, W. Higgins, J. Janowiak, K.C. Mo, C. Ropelewski, J. Wang, A. Leetma, R. Reynolds, R. Jenne, and D. Joseph, The NCEP/NCAR 40-year reanalysis project, *Bullet. Amer. Meteorol. Soc.*, *77*, 437-471, 1996.
Kanakidou, M., J.H. Seinfeld, S.N. Panis, L. Barnes, F.J. Dentener, M.C. Facchini, R.V. Dingenen, E. Ervens, A. Nenes, C.J. Nielsen, E. Swietlicki, J.P. Putaud, Y. Balkanski, S. Fuzzi, J. Horth, G.K. Moortgat, R. Winterhalter, C.E.L. Myhre, K. Tsigaridis, E. Vignati, E.G. Stephanou, and J. Wilson, Organic aerosol and global climate modeling: a review, *Atmos. Chem. Phys.*, *5*, 1053-1123, 2005.
Kauffman, J.B., M.D. Steele, D.L. Cummings, and V.J. Jaramillo, Biomass dynamics associated with deforestation, fire, and conversion to cattle pasture in a Mexican tropical dry forest, *Forest Ecology and Management*, *176*, 1-12, 2003.
Kaufman, Y., J., D. Tanre, and O. Boucher, A satellite view of aerosols in climate systems, *Nature*, *419*, 215-223, 2002.
Kotchenruther, R.A., and P.V. Hobbs, Humidification factors of aerosols from biomass burning in Brazil, *J. Geophys. Res.*, *103*, 32,081-32,089, 1998.
Kreidenweis, S.M., L.A. Remer, R. Bruintjes, and O. Dubovik, Smoke aerosols from biomass burning in Mexico: Hygroscopic smoke optical model, *J. Geophys. Res.*, *106*, 4831-4844, 2001.
Koren, I., Y.J.Kaufman, L.A.Remer, and J.V. Martins, Measurement of the effect of Amazon smoke on inhabitation of cloud formation, science, *Science*, *303*, 1342-1345, 2004.
Lavoue, D., C.Liousse, H.Cahchier, B.J.Stocks, and J.G.Goldammer, Modeling of carbonaceous particles emitted by boreal and temperate wildfires at northern latitudes, *J. Geophys. Res.*, *105*, 26,871-26,890, 2000.
Levinson, D.H., and A.M. Waple(eds), State of the climate in 2003, *Bull. Amers. Meteoro. Soc.*, *85*, S1-S72, 2004.
Liousse, C., J.E. Penner, C.C.Chuang, J.J. Walton, and H. Eddleman, A global three dimensional model study of carbonaceous aerosols, *J. Geophsy. Res.*, *101*, 19,441-19,432, 1996.
Malm, W.C., J.F. Sisler, D. Huffman, R.A. Eldred, and T.A. Cahill, Spatial and seasonal trends in particle concentration and optical extinction in the United States, *J. Geophys. Res.*, *99*, 1357-1370, 1994.
Malm, W.C., B.A.Schichtel, M.L.Pitchford, L.L.Ashbaugh, and R.A.Eldred, Spatial and monthly trends in speciated fine particle concentration in the United States, *J. Geophys. Res.*, *109*, doi:10.1029/2003JD003739, 2004.

Mellor, G.L., and T. Yamada, A hierarchy of turbulent closure models for planetary boundary layers, *J. Atmos. Sci.*, *31*, 1791-1806, 1974.
Pielke, R.A., R.L. Walko, J.L. Eastman, W.A. Lyons, R.A. Stocker, M. Uliasz, and C.J. Tremback, A comprehensive meteorological modeling system - RAMS, *Meteor. Atmos. Phys.*, *49*, 69-91, 1992.
Park, R.J., D.J.Jacob, M.Chin, and R.V.Martin, Sources of carbonaceous aerosols over the United States and implications for natural visibility, *J. Geophys. Res.*, *108*, doi:10.1029/2002JD003190, 2003.
Penner, J.E., R. Dickinson, and C. O'Nell, Effects of aerosol from biomass burnig on the global radiation budget, *Scinces*, *256*, 1423-1434, 1992.
Peppler, R.A., C.P. Bahrmann, J.C. Barnard, J.R. Campbell, M.-D. Cheng, R.A. Ferrare, R.N. Halthore, L.A. Heilman, D.L. Hlavka, N.S. Laulainen, C.-J. Lin, J.A. Ogren, M.R. Poellot, L.A. Remer, K. Sassen, J.D. Spinhirne, M.E. Splitt, and D.D. Turner, ARM Southern Great Plains Site Observations of the Smoke Pall Associated with the 1998 Central American Fires, *Bull. Amer. Meteor. Soc.*, *81*, 2563–2592, 2000.
Prins, E.M., J.M. Feltz, W.P. Menzel, and D.E. Ward, An overview of GOES-8 diurnal fire and smoke results for SCAR-B and the 1995 fire season in South America, *J. Geophys. Res.*, *103*, 31,821-31,835, 1998.
Pruppacher, H.R., and J.D. Klett, *Microphysics of clouds and precipitation*, 714 pp., D. Reidel Publishing Company, Dordrecht, Holland, 1978.
Reid, J.S., P.V.Hobbs, R.J.Ferek, D.R.Blake, J.V.Martins, M.R.Dunlap, and C.Liousse, Physical, chemical, and optical properties of regional hazes dominated by smoke in Brazil, *J. Geophys. Res.*, *103*, 32,059-32,080, 1998.
Reid, J.S., and P.V.Hobbs, Physical and optical properties of young smoke from individual biomass fires in Brazil, *J. Geophys. Res.*, *103*, 32,013-32,030, 1998.
Reid, J.S., E.M. Prins, D.L. Westphal, C.C. Schmidt, K.A. Richardson, S.A. Christopher, T.F. Eck, E.A. Reid, C.A. Curtis, and J.P. Hoffman, Real-time monitoring of South American smoke particle emissions and transport using a coupled remote sensing/box-model approach, *Geophys. Res. Lett.*, *31*, doi:10.1029/2003GL018845, 2004.
Reid, J.S., R.Koppmann, T.F.Eck, and D.P.Eleuterio, A review of biomass burning emissions, part II: intensive physical properties of biomass burning particles, *Atmos. Chem. Phys.*, *5*, 799-825, 2005a.
Reid, J.S., T.F. Eck, S.A. Christopher, R.Koppmann, O.Dubovik, D.P. Eleuterio, B.N. Holben, E.A. Reid, and J.Zhang, A Review of Biomass Burning Emissions Part III: Intensive Optical Properties of Biomass Burning Particles, *Atmos. Chem. Phys.*, *4*, 5201-5260, 2005b.
Ryerson, T.B., et al., Effect of petrochemical industrial emissions of reactive alkenes and NOx on tropospheric ozone formation in Houston, Texas, *J. Geophys. Res.*, *108*, doi:10.1029/2002JD003070, 2003.
Robock, A., Enhancement of surface cooling due to forest fire smoke, *Science*, *242*, 911-913, 1988.
Rogers, C.M., and K.P. Bowman, Transport of smoke from the Central American fires of 1998, *J. Geophys. Res.*, *106*, 28,357-28,368, 2001.
Russel, M., and D.T. Allen, Seasonal and spatial trends in primary and secondary organic carbon concentrations in southeast Texas, *Atmospheric Environment*, *38*, 3225-3239, 2004.

Schmid, H., L. Laskus, H.J. Abraham, U. Balternsperger, V. LAvanchy, M. Bizjak, P. Burba, H. Cachier, D. Crow, J. Chow, T. Gnauk, A. Even, H.M.t. Brink, K.-P. Giesen, R. Hitzenberger, C. Hueglin, W. Maenhaut, C. Pio, A. Carvalho, J.-P. Putaud, D. Toom-Sauntry, and H. Puxbaum, Results of the "carbon conference" international aerosol carbon round robin test stage I, *Atmospheric Enviroment*, *35*, 2111-2121, 2001.

Slinn, S.A., and W.G.N. Slinn, Predictions for particle deposition on natural waters, *Atmos. Environ.*, *14*, 1013-1016, 1980.

Slinn, W.G.N., Precipitation scavenging, in *Atmospheric Science and Power Production*, edited by D. Danderson, pp. 466-532, Tech. Inf. Cent. Off. of Sci. and Techn. Inf., Dep. of Energy, Washington, D.C., 1984.

Schell, B., I.J.Ackermann, H.Hass, F.S.Binkowski, and A.Ebel, Modeling the formation of secondary organic aerosol within a comprehensive air quality model, *J.Geophys.Res.*, *106*, 28,275-28,293, 2001.

Schmid, B., R.Ferrare, C.Flynn, R.Elleman, D.Covert, A.Strawa, E.Welton, D.Turner, H.Jonsson, J.Redemann, J.Eliers, K.Ricci, A.G.Hallar, M.Clayton, J.Michalsky, A.Smirnov, B.Holben, and J.Barnard, How well can we measure the vertical profile of tropical aerosol extinction?, *J. Geophys. Res.*, 2005, submitted.

Strader, R., F.Lurmann, and S.N.Panis, Evaluation of secondary organic aerosol formation in winter, *Atmospheric Environment*, *33*, 4849-4863, 1999.

Stull, R.B., An Introduction to Boundary Layer Meteorology, *Kluwer Academic Publishers*, pp.666, 1989.

Takemura, T., H. Okamoto, Y. Maruyama, A. Numaguti, A. Higurashi, and T. Nakajima, Global three-dimensional simulation of aerosol optical thickness distribution of various origins, *J. Geophys. Res.*, *105*, 17,853-17,873, 2000.

Tanner, R.L., W.J. Parkhurst, M.L.Valente, K.L.Humes, K.Jones, and J.Gilbert, Impact of the 1998 Central American fires on PM2.5 mass and composition in the southeastern United States, *Atmospheric Environment*, *35*, 6539-6547, 2001.

Tegen, I., P. Hollrig, M. Chin, I. Fung, D. Jacob, and J. Penner, Contribution of different aerosols to the global aerosol extinction optical thickness: estimates from model results, *J. Geophys. Res.*, *102.*, 23,895-23,915, 1997.

Trentmann, J., M.O. Andreae, H.-F. Graf, P.V. Hobbs, R.D. Ottmar, and T. Trautmann, Simulation of a biomass-burning plume: comparison of model results with observations, *J. Geophys. Res.*, *107*, doi:10.1029/2002JD000410, 2002.

Tropp, R.J., S.D.Kohl, J.C.Chow, and C.A.Frazier, Final report for the Texas PM2.5 sampling and analysis study, prepared for Bureau of air quality control, City of Houston, TX, Documet No.6570-685-7770.1F, Prepared by Desert Research Institute, available at http://eosweb.larc.nasa.gov/GUIDE/dataset_documents/narsto_texas_guide.html, 1998.

Turco, R.P., and F.Yu, Particle size in an expanding plume undergoing simultaneous coagulation and condensation, *J. Geophys. Res.*, *104*, 19,227-19,241, 1999.

Turpin, B.J., P.Saxena, and E.Andrews, Measuring and simulating particulate organics in the atmosphere: problems and prospects, *Atmospheric Environment*, *34*, 2983-3013, 2000.

Turpin, B.J., and H.-J. Lim, Species contributions to $PM_{2.5}$ mass concentration: revisiting common assumptions for estimating organic mass, *Aerosol Science and Technology*, *35*, 602-610, 2001.

Twomey, S., The influence of pollution on the shortwave albedo of clouds, *J. Atmos. Sci.*, *34*, 1149-1152, 1977.

Uno, I., G.R.Carmichael, D.G.Streets, Y.Tang, J.J.Yienger, S.Satake, Z.Wang, J.-H. Woo, S.Guttikunda, M.Uematsu, K.Matsumoto, H.Tanimoto, K.Yoshioka, and T.Iida, Regional chemical weather forecasting system CFORS: Model description and analysis of surface observations at Japanese island stations during the ACE-Asia experiment, *J.Geophys.Res.*, *108*, doi:10.1029/2002JD002845, 2003.

Walko, R.L., W.R. Cotton, M.P. Meyers, and J.Y. Harrington, New RAMS cloud microphysics parameterization, part I: The single-moment scheme, *Atmos. Res.*, *38*, 29-62, 1995.

Walko, R.L., L.E. Band, J. Baron, T.G.F. Kittel, R. Lammers, T.J. Lee, R.A. Pielke, C. Tague, C. Taylor, C.J. Tremback, and P.L. Vidale, Coupled Atmosphere-Biophysics-Hydrology models for environmental Modeling, *J Appl Meteorol.*, *39*, 931-944, 2000.

Watson, J.G., J.C.Chow, H.Moosmuller, M.Green, N.Frank, and M.Pitchfort, Guidance for using continuous mintors in PM2.5 monitoring networks, *Office of Air Quality Planning and Standards, U.S. Envirometal Protection Agency, EPA-454/R-98-012*, 1998.

Wang, J., U. Nair, and S.A. Christopher, GOES-8 Aerosol optical thickness assimilation in a mesoscale model: Online integration of aerosol radiative effects, *J. Geophys. Res.*, *109*, doi:10.1029/2004JD004827, 2004.

Westphal, D.L., and O.B. Toon, Simulation of microphysical, radiative, and dynamical processes in a continental-scale forest smoke plume, *J. Geophys. Res.*, *96*, 22,379-22,400, 1991.

Yu, S., R.L.Dennis, P.V.Bhave, and B.K.Eder, Primary and secondary organic aerosols over the United States: estimates on the basis of observed organic carbon (OC) and elemental carbon (BC), and air quality modeled primary OC/EC ratios, *Atmospheric Environment*, *38*, 5257-5268, 2004.

Zhang, L., S.Gong, J.Padro, and L.Barrie, A size-segregated particle dry deposition scheme for an atmospheric aerosol module, *Atmospheric Enviroment*, *35*, 549-560, 2001.

Zhang, Y., B.Pun, K.Vijayaraghavan, S-Y.Wu, C.Seigneur, S.N.Panis, M.Z.Jacobson, A.Nenes, and J.H.Seinfeld, Development and application of the model of aerosol dynamics, reaction, ionization, and dissolution, *J. Geophys. Res.*, *109*, doi:10.1029/2003JD003501, 2004.

Tables and Figures

Table Caption:

Table 1: Location and site names of nine IMPROVE monitoring stations.

Table 2: Comparison statistics between measured quantities (Y) and modeled smoke concentration (X) in different simulation experiments (see text for details). N: number of comparison pairs; R: linear correlation coefficient. Also shown is the best liner fit equation and averaged smoke concentration in each comparison.

Figure Caption:

Figure 1. Model domain where the rectangle with dotted lines shows the domain of fine-grid. Also overlaid is the map of gray-coded total smoke emission (1Gg = 10^9g) from FLAMBE database during April 20 to May 21, 2003. The black square denotes location of ARM Southern Great Plains (SGP) site, and open circles with different numbers represent the locations of the nine IMPROVE sites (see table 1 for details).

Figure 2. Time series of $PM_{2.5}$ mass concentration in various ground-based stations in the state of Texas. The inlet map in each panel shows the location of the corresponding station in Texas. The horizontal doted lines in each panel outline the air quality categories based on the EPA 24-hour standard, e.g., $PM_{2.5}$ mass (in μgm^{-3}) of 15.4, 40.4, 65.4, 150.4, 250.4, 500.4 are upper limits for the categories of good, moderate, unhealthy for special groups (e.g., elderly and children), unhealthy, very unhealthy and hazardous, respectively. The shaded background in different time intervals highlights the time frames of four major smoke events (see text for details).

Figure 3. (a)-(d): MODIS true color images from Terra and Aqua satellites during May 9 – May 12, 2003 of smoke plumes transiting from Yucatan peninsular along the Gulf coast of Mexico to the SEUS. Red dots indicate the location of fires (image courtesy: MODIS Rapid Response System). Note these images are not geographically projected. Sunglint and smoke regions have been denoted. (e): Modeled dry smoke concentration near the surface on 1800UTC May 9 2003. Solid dots show the locations of different $PM_{2.5}$ observation sites and are color-coded based on air quality categories. Red arched lines on show the TECQ best estimate of smoke (see text for details). Pink contour lines are the geopotential heights at 700hpa. Letters H and L locate the major high and low pressure systems. (f) (g) and (h): same as (e) but for May 10, May 11 and May 12, respectively. Note in panel (g), $PM_{2.5}$ data was only available in Texas.

Figure 4. (a)-(c) Time series of aerosol extinction coefficient (km^{-1}) profiles at 335nm derived from lidar measurements at ARM SGP site on May 9, 10, and 11 2003 respectively. (d)-(f) are same as (a)-(c) but shows the profile of modeled smoke mass concentration.

Figure 5. The map of correlation coefficients between daily-averaged modeled smoke concentration near the surface with the measured $PM_{2.5}$ concentration at different $PM_{2.5}$ sites in Texas.

Figure 6. (a) Comparison between daily-averaged modeled smoke concentrations (x-axis) near the surface with the measured $PM_{2.5}$ concentration (y-axis) near the surface at 34 $PM_{2.5}$ observation sites in state of Texas. (b)-(i) same as (a) but at different individual site (black square in the inlet map). Also shown in each panel are the correlation coefficient (R), the significance level of correlation (P, not significant when P greater than 0.05), number of comparison pairs (N), root mean square error (RMSE), mean and standard deviation of both modeled and measured quantities.

Figure 7. Panel (A)-(I): time series of modeled smoke mass concentration (SMK, continuous line) and the measured concentration of total carbon (TC, red dots) in different IMPROVE sites. Also shown are the correlation coefficient R between these two variables as well as the mean and standard deviation of each variable. The locations of each IMPROVE stations corresponding to (A)-(I) are shown in panel (J).

Figure 8. Comparison of modeled smoke concentration (x-axis) from RAMS-AROMA baseline simulation with the measured mass concentrations of (a) KNON and (b) total carbon at three IMPROVE sites (SIKE, CACR and UPBU). (c) and (d) are same as (b) except that the modeled smoke concentration are from simulations with 1.5 and 2.0 of baseline smoke emissions, respectively.

Figure 9. (a) Averaged mass concentration of $PM_{2.5}$, carbon and sulfate aerosols at IMPROVE site, SIKE LA in two time periods, one in April - May of 2000 - 2002 and another in smoke days during April 20 – May 20 2003. Also shown in the first time period is the mass percentage of carbon and sulfate aerosols relative to the $PM_{2.5}$ mass concentration. In the second time period, only the increased percentages (with plus sign) of $PM_{2.5}$, carbon and sulfate mass relive to their corresponding values in the first time period are shown. See text for details. (b) and (c) are same as (a) but for CACR AR and UPBU AR, respectively. The numbers in the bracket of each panel show respectively the latitude and longitude of that IMPROVE site.

Figure 10. Measured column AOT (blue dots) and modeled smoke AOT (lines in pink) at the ARM SGP site. The measured AOT at 0.55μm is derived from the logarithmic fit between NIMFR AOT at 0.50μm and 0.61μm. Bars in blue and green colors show the daily-averaged AOT and Angstrom exponents derived from the ground-based AOT measurements, respectively. Solid, dashed, and dot-dashed (pink) lines represent modeled AOT for baseline smoke emission, 1.5 baseline, and 2.0 baseline emission, respectively.

Figure 11. The frequency distribution of correlation coefficients between modeled smoke and measured $PM_{2.5}$ concentration at 36 stations in Texas for simulations with hourly and with daily emission, respectively.

Figure 12. Diurnal variation of model-simulated AOT in the smoke source region. The AOT at each hour is computed by averaging the AOTs at that hour in 30 days.

Table 1: Location and site names of nine IMPROVE monitoring stations.

Site name	Location	Latitude (N)	Longitude (W)
BIBE	Big Band National Park, Texas	29.30	103.12
GUMO	Guadalupe Mountains, Texas	31.83	104.81
SAFO	Sac and Fox, Kansas	39.98	95.57
TALL	Tallgrass, Kansas	38.30	96.60
SIPS	Sipsy Wilderness, Alabama	34.34	87.34
BRET	Brenton, Louisiana	29.12	89.21
SIKE	Sikes, Louisiana	32.06	92.43
CACR	Caney Creek, Arkansas	34.45	94.14
UPUC	Upper Buffalo Wilderness, Arkansas	35.83	93.20

Table 2. Comparison statistics between measured quantities (Y) and modeled smoke concentration (X) in different simulation experiments (see text for details). N: number of comparison pairs; R: linear correlation coefficient. Also shown is the best liner fit equation and averaged smoke concentration in each comparison.

Measured Quantity	Experiments	N	R	Linear equation	Modeled smoke (μgm^{-3})
IMPROVE carbon	Layer8-Hourly-1.0E	30	0.74	Y = 0.67X + 1.37	2.01 ± 1.55
	Layer8-Daily-1.0E	30	0.77	Y = 0.66X + 1.30	2.15 ± 1.63
	Layer7-Hourly-1.0E	30	0.70	Y = 0.61X + 1.42	2.13 ± 1.61
	Layer9-Hourly-1.0E	30	0.75	Y = 0.74X + 1.41	1.77 ± 1.42
IMPROVE KNON	Layer8-Hourly-1.0E	30	0.69	Y = 32.80X + 6.63	2.01 ± 1.55
	Layer8-Daily-1.0E	30	0.77	Y = 34.39X - 1.32	2.15 ± 1.63
	Layer7-Hourly-1.0E	30	0.63	Y = 28.61X + 11.45	2.13 ± 1.61
	Layer9-Hourly-1.0E	30	0.72	Y = 37.10X + 6.67	1.77 ± 1.42
PM2.5 in 34 stations in Texas	Layer8-Hourly-1.0E	1005	0.76	Y = 2.90X + 9.15	3.02 ± 2.90
	Layer8-Daily-1.0E	1005	0.78	Y = 2.56X + 8.69	3.61 ± 3.42
	Layer7-Hourly-1.0E	1005	0.75	Y = 2.50X + 9.40	3.40 ± 3.35
	Layer9-Hourly-1.0E	1005	0.75	Y= 3.56X + 0.02	2.50 ± 2.35

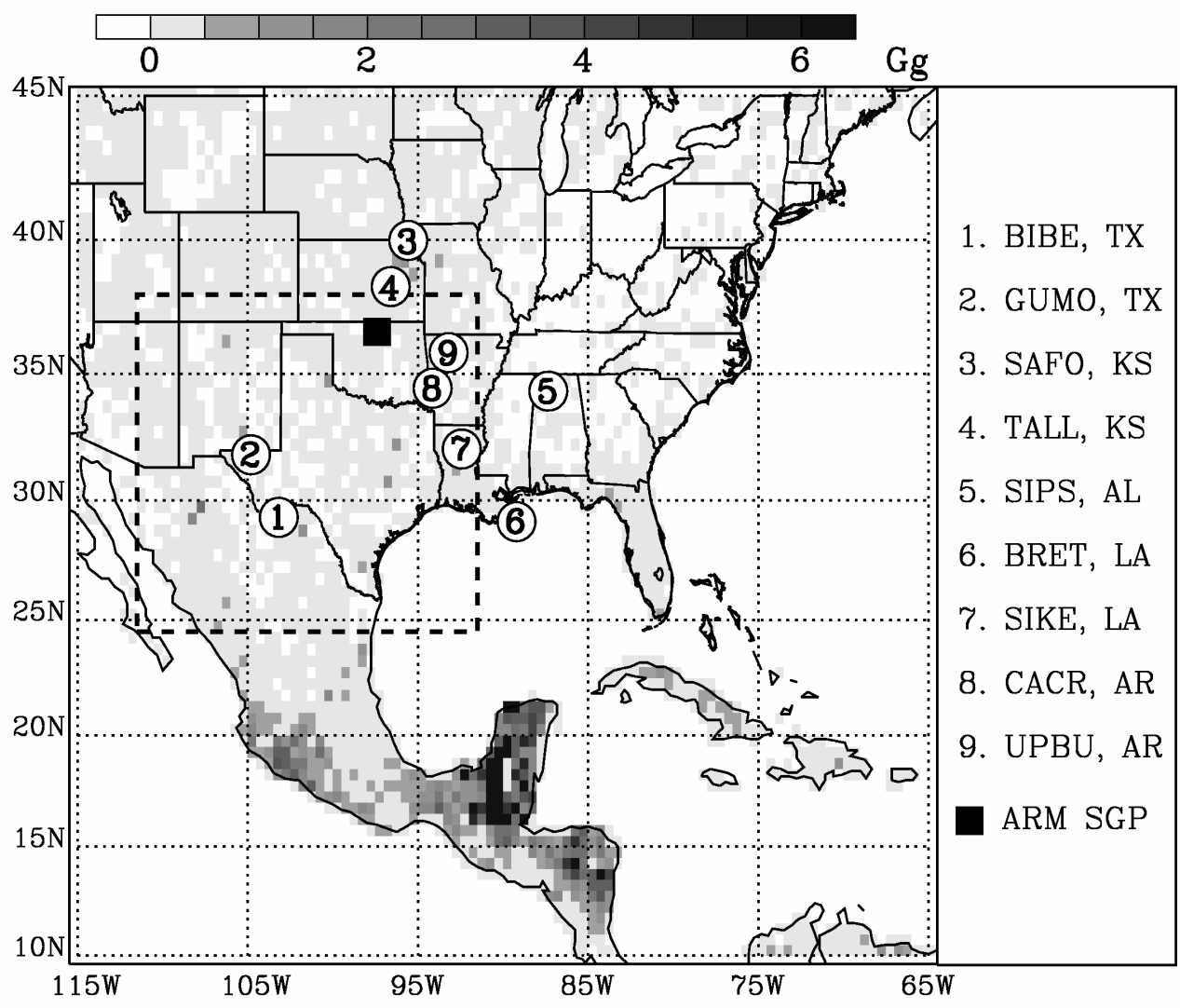

Figure 1. *Wang et al.*, 2005.

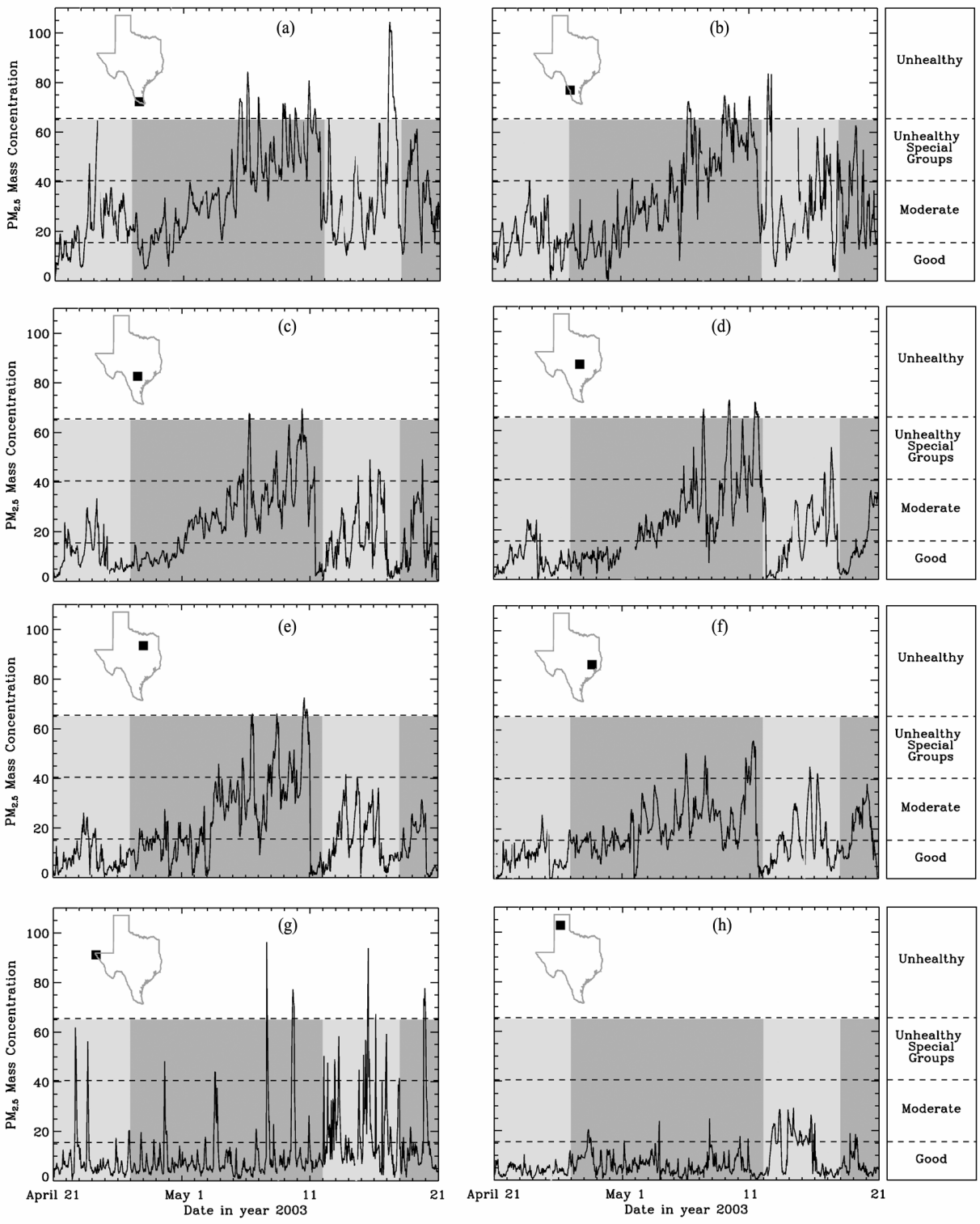

Figure 2. *Wang et al.*, 2005.

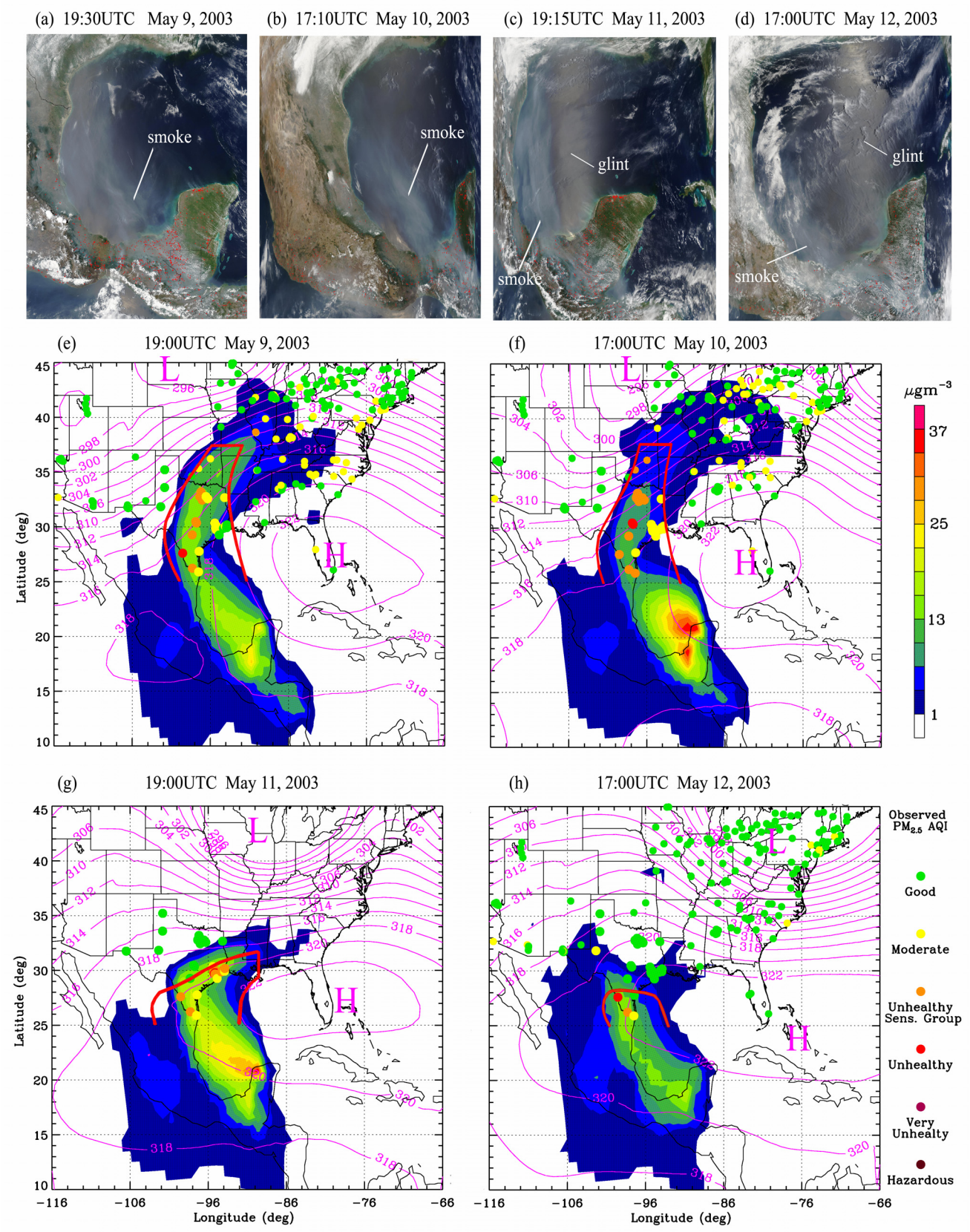

Figure 3. *Wang et al.*, 2005.

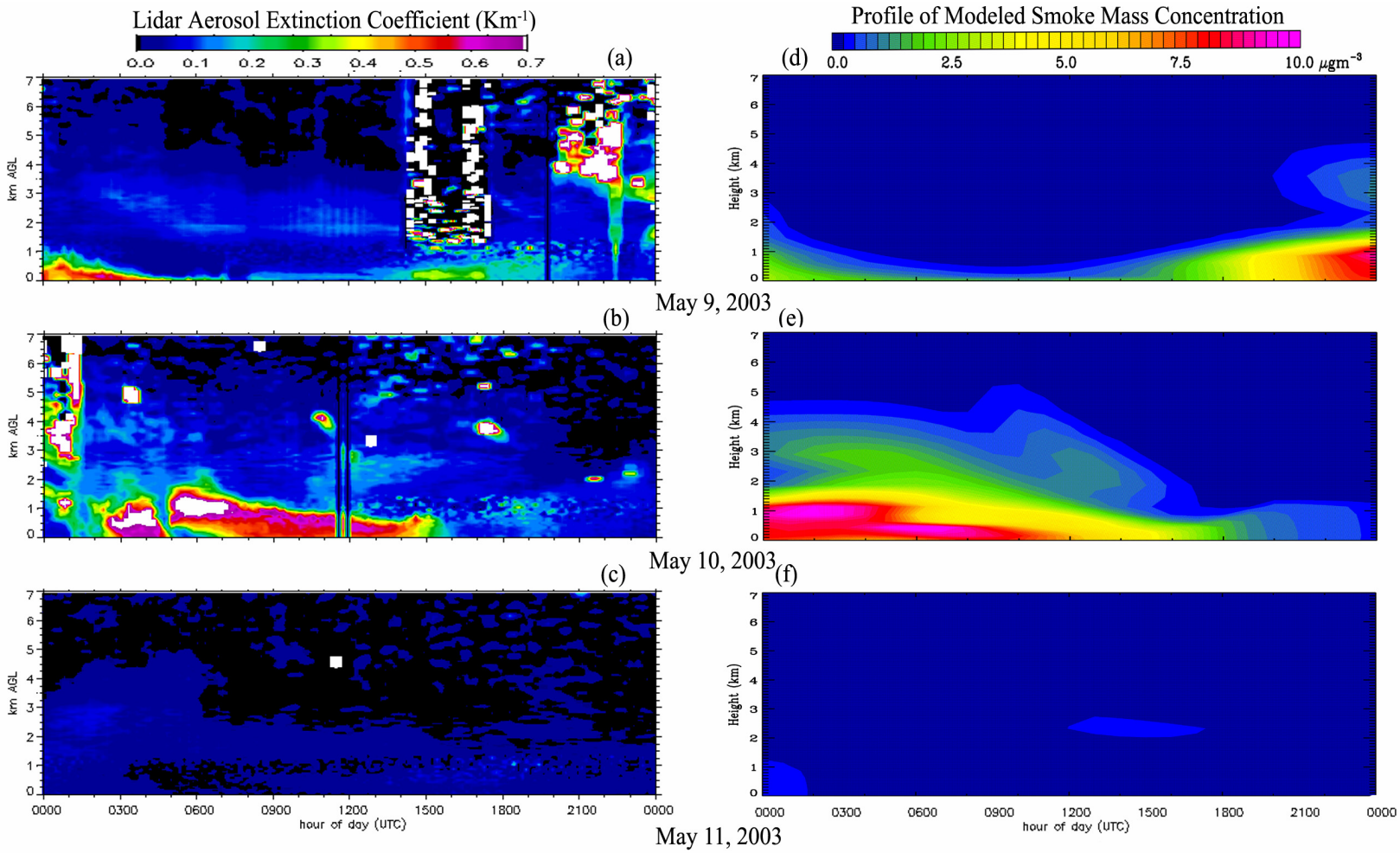

Figure 4. *Wang et al.*, 2005.

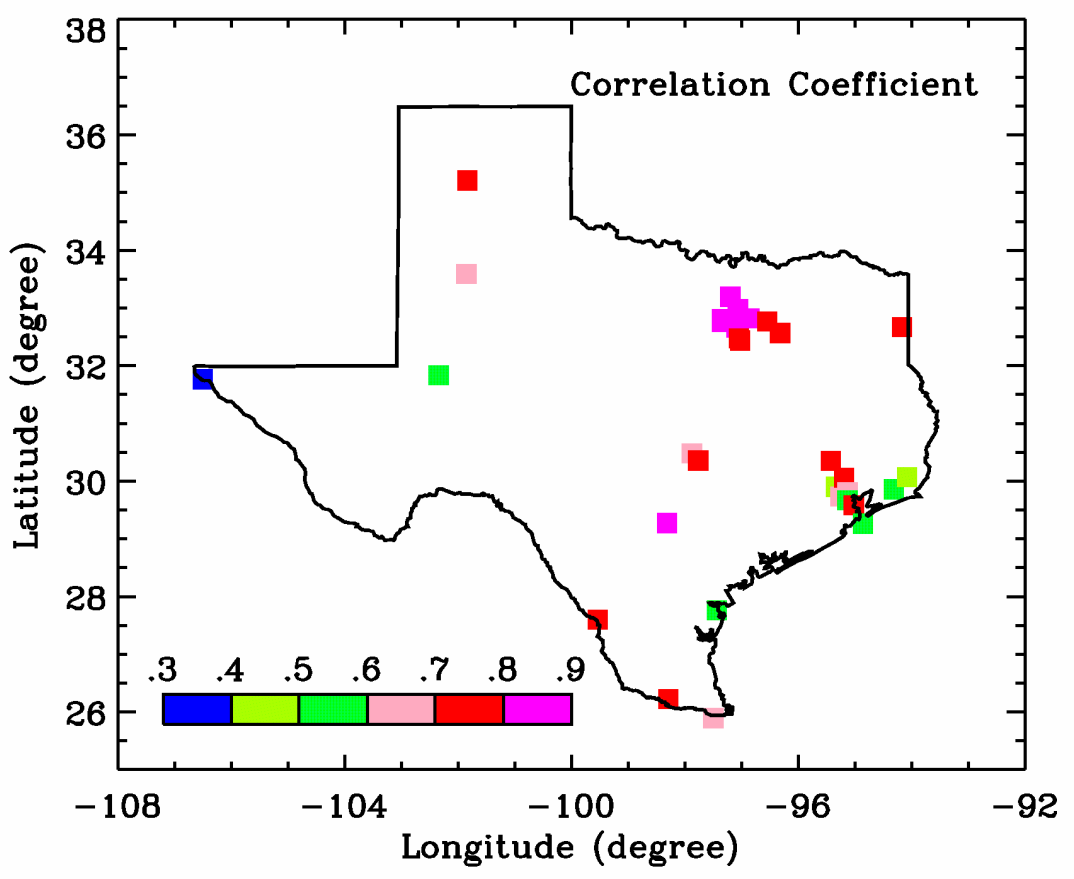

Figure 5. *Wang et al.*, 2005.

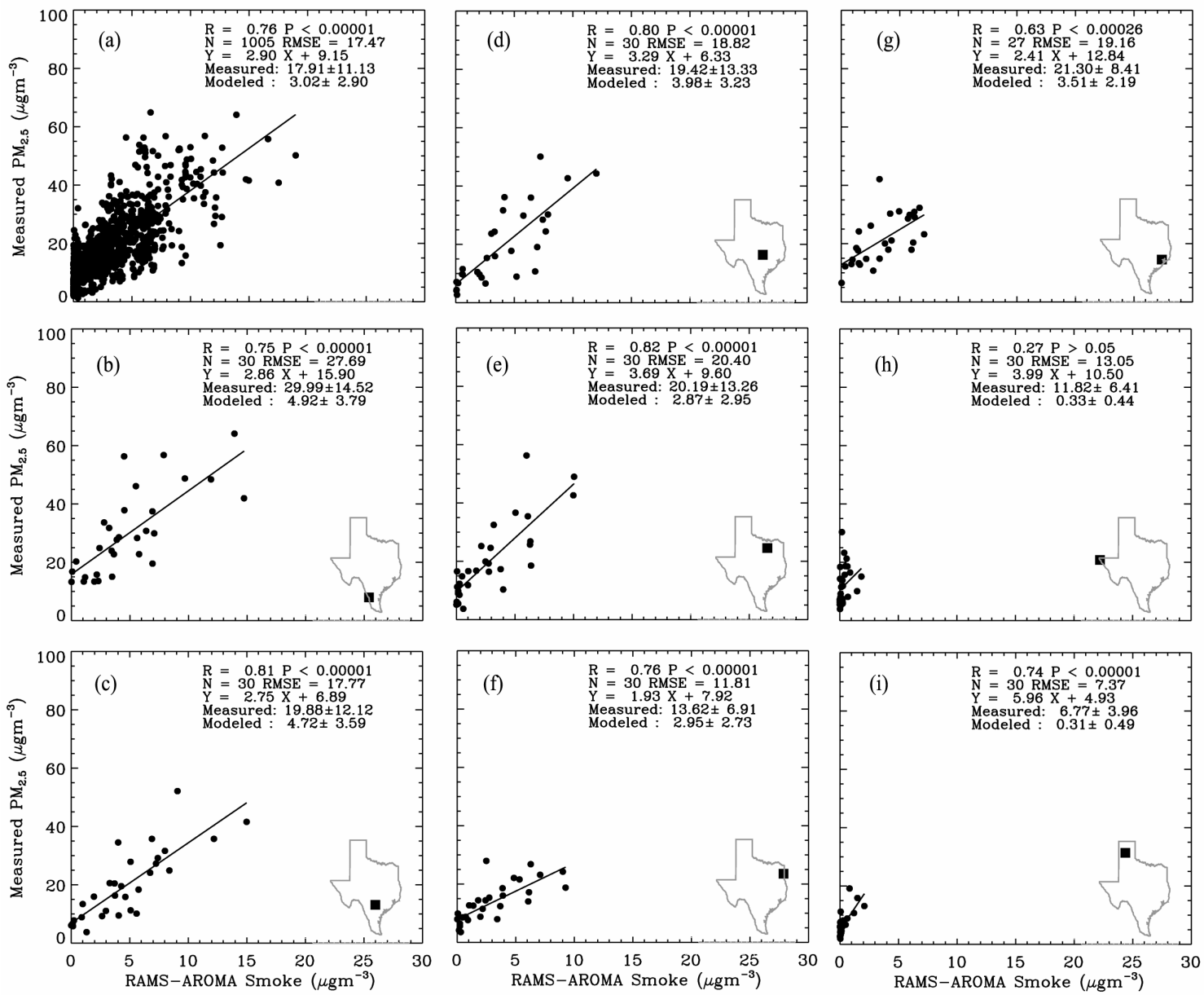

Figure 6. *Wang et al.*, 2005.

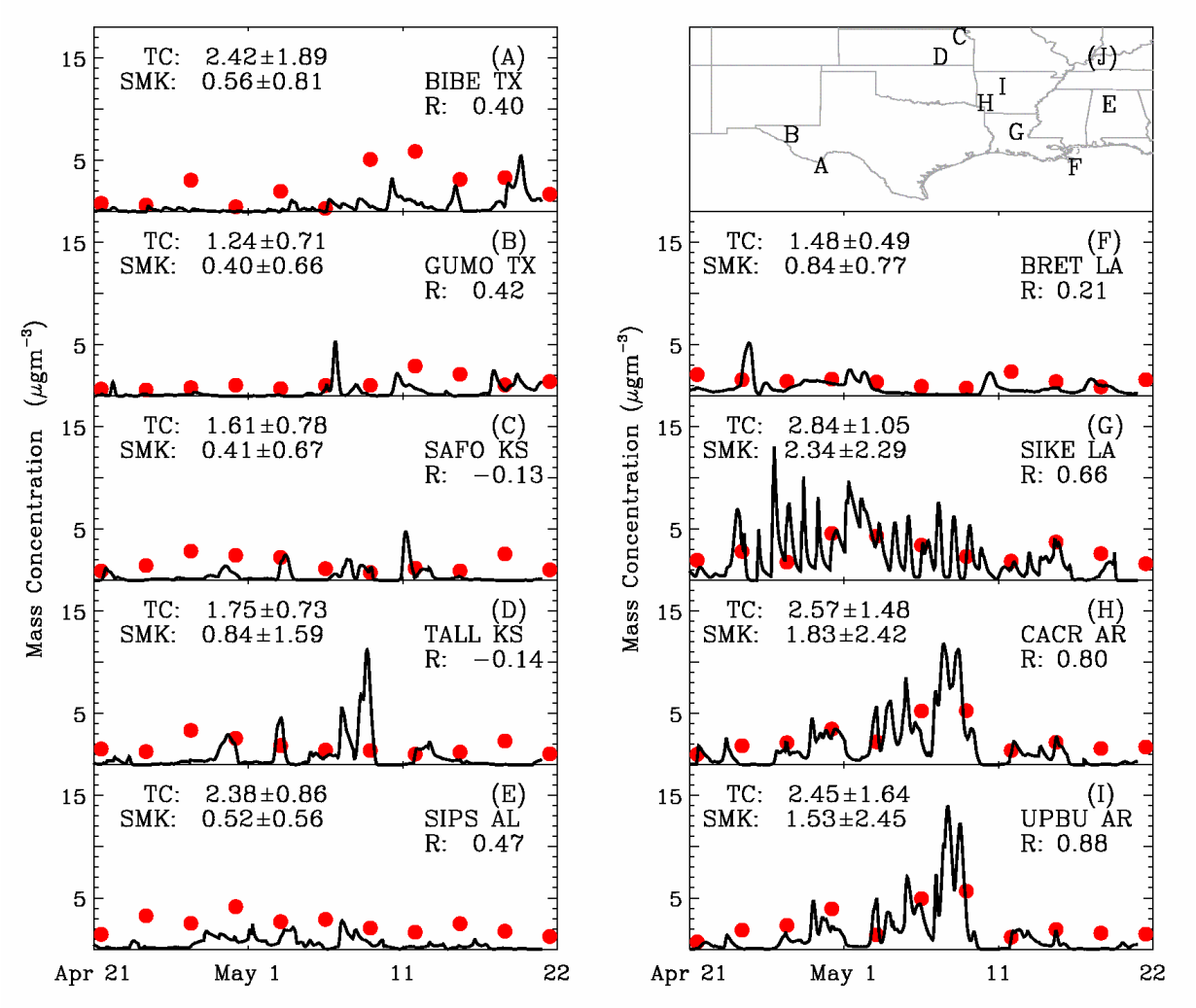

Figure 7. *Wang et al.*, 2005.

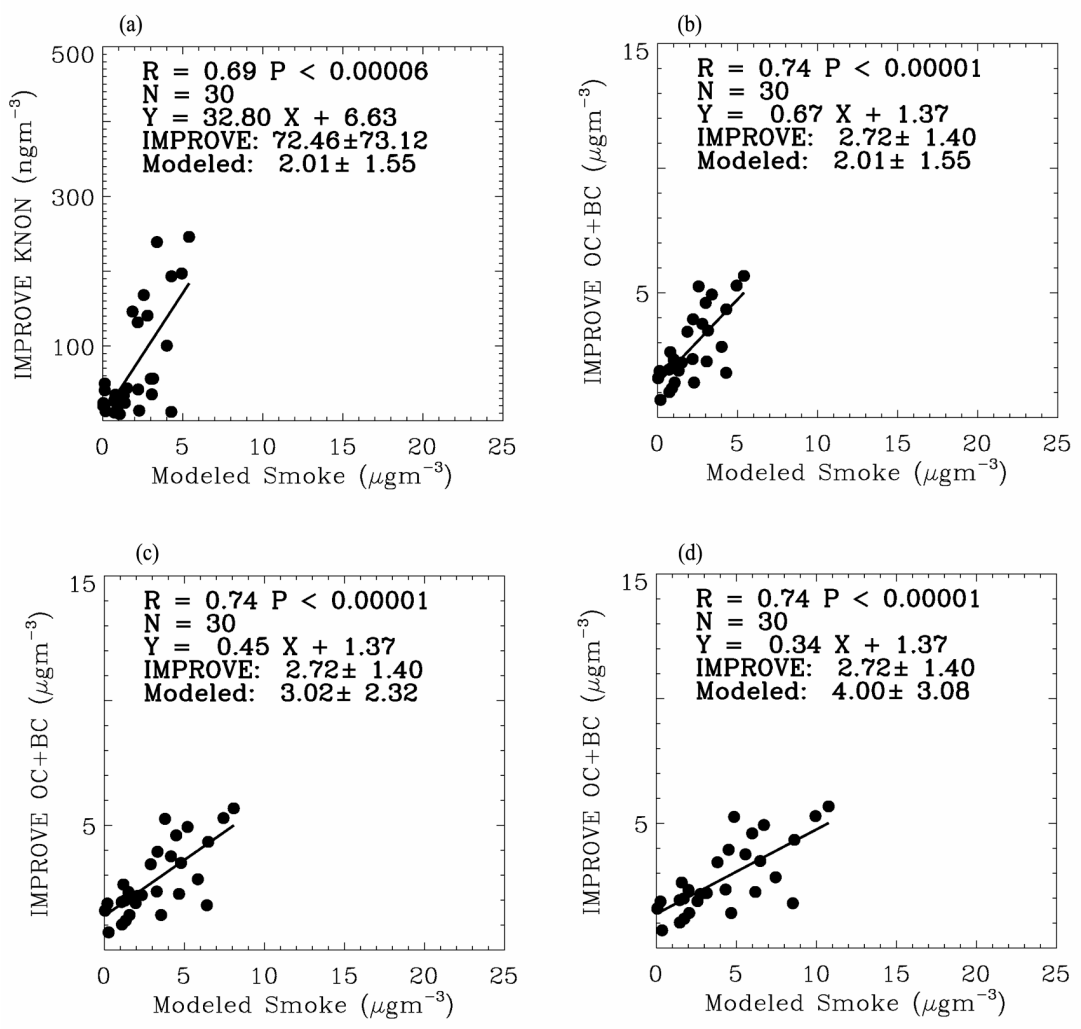

Figure 8. *Wang et al.*, 2005.

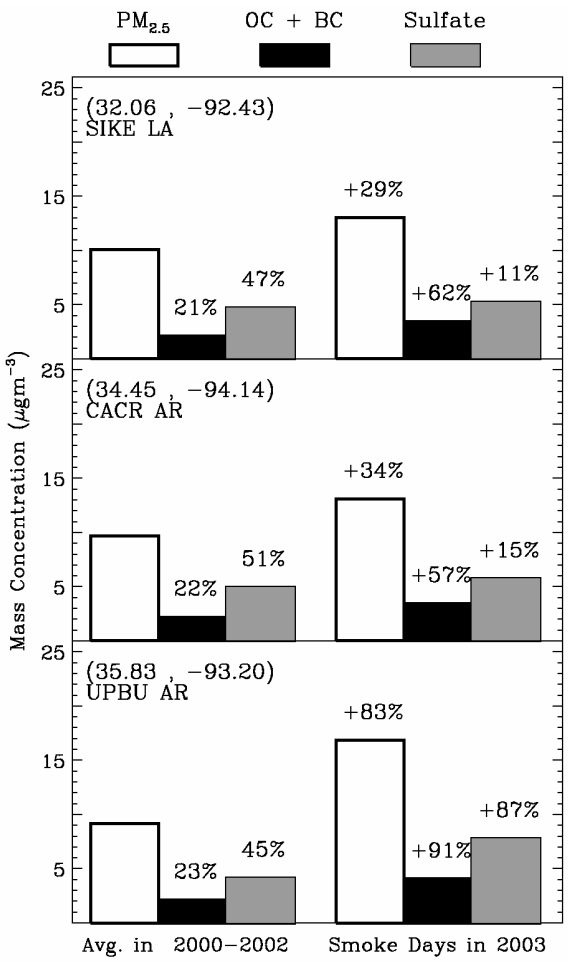

Figure 9. *Wang et al.*, 2005.

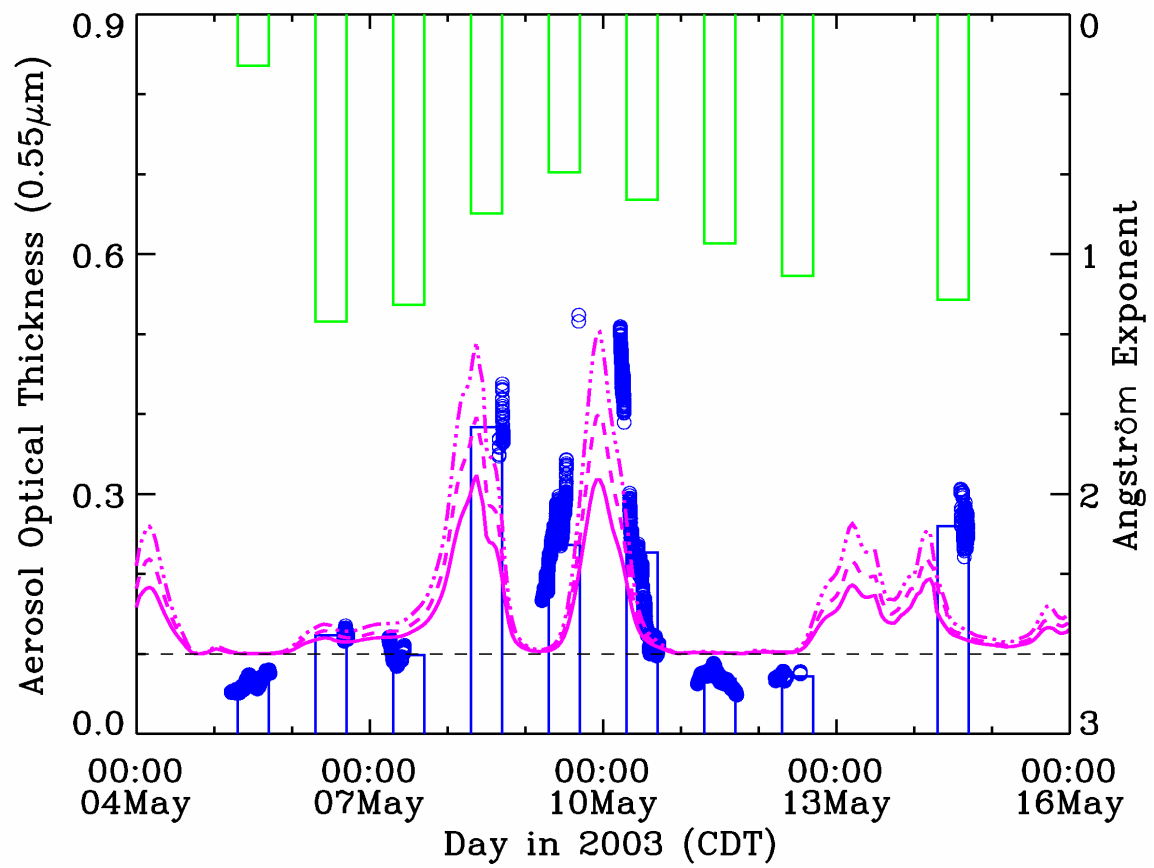

Figure 10. *Wang et al.*, 2005.

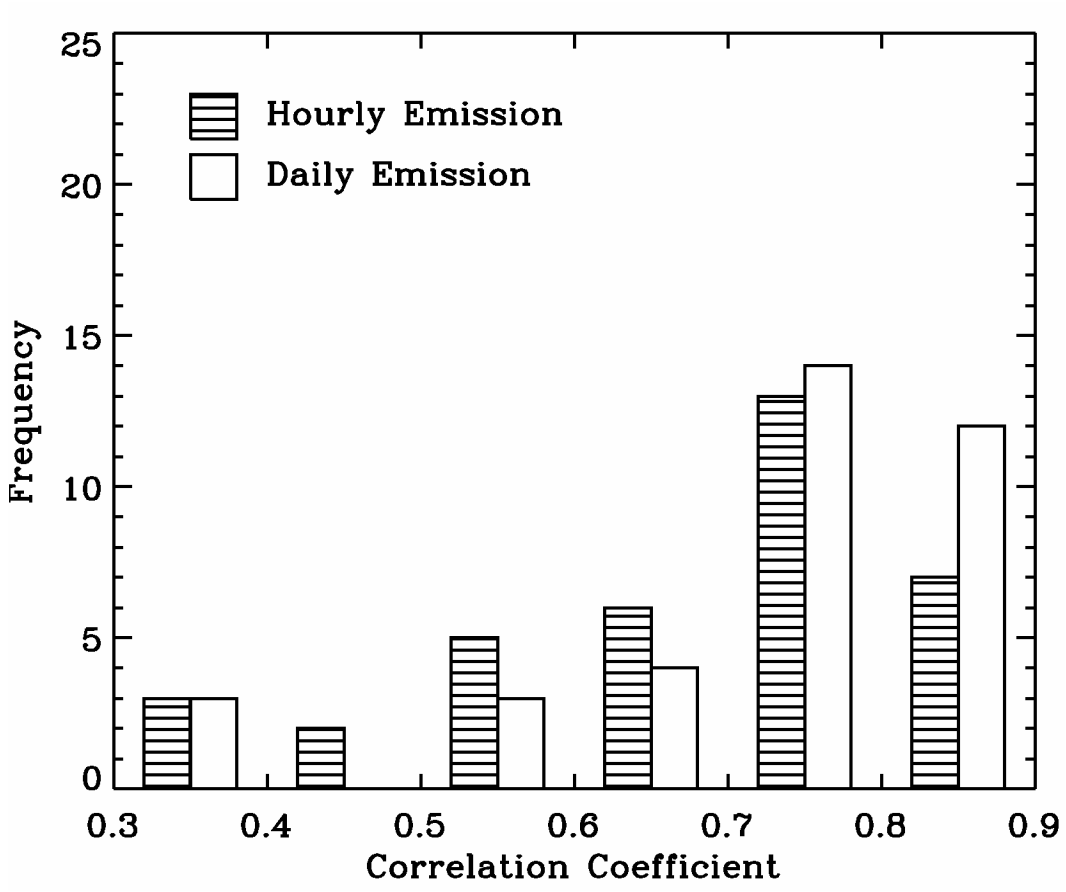

Figure 11. *Wang et al.*, 2005.

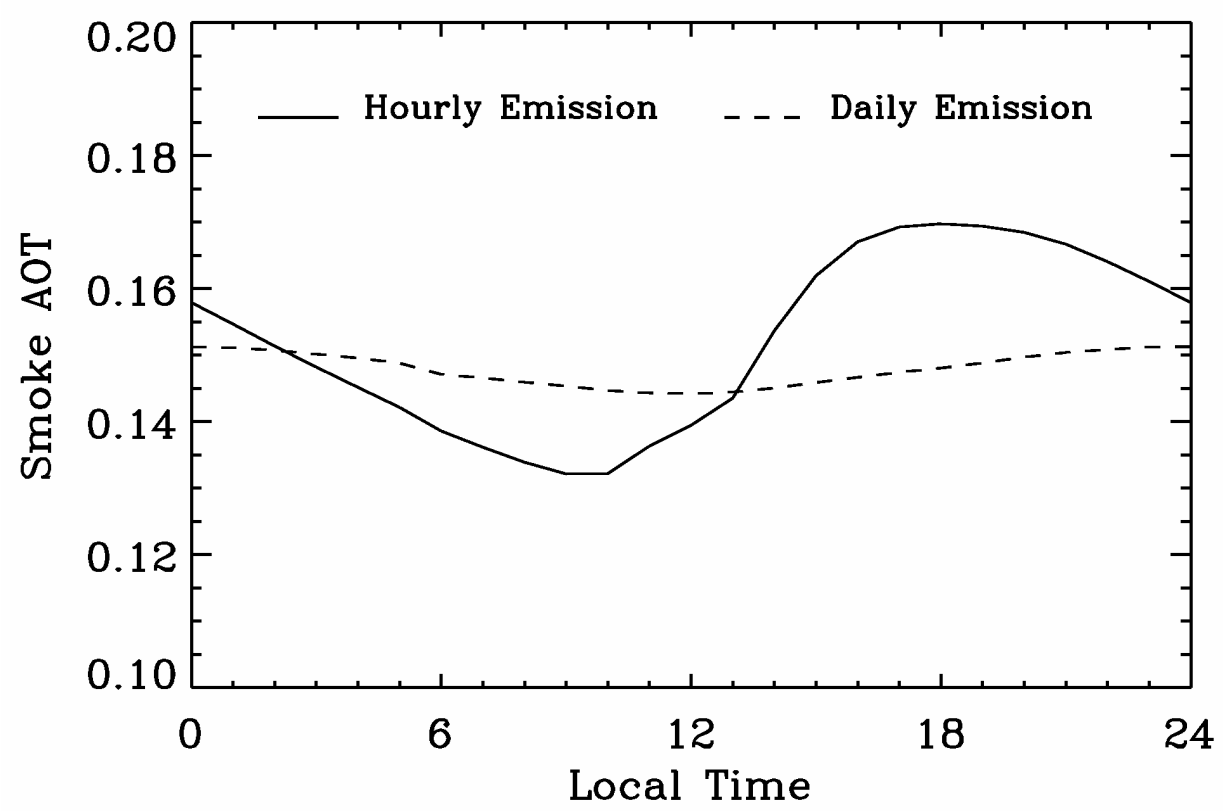

Figure 12. *Wang et al.*, 2005.